Title:

EBF1 limits the numbers of cochlear hair and supporting cells and forms the scala tympani and spiral limbus during inner ear development

Abbreviated title: EBF1 controls the development of the cochlea

Author names:

Hiroki Kagoshima[1], Hiroe Ohnishi[1], Ryosuke Yamamoto[2], Akiyoshi Yasumoto[1], Yosuke Tona[1], Takayuki Nakagawa[1], Koichi Omori[1], and Norio Yamamoto[1,3]

[1]Department of Otolaryngology, Head and Neck Surgery, Graduate School of Medicine, Kyoto University, Kyoto, Japan

[2]Biological Sciences, Sunnybrook Research Institute, Sunnybrook Health Sciences Centre, Toronto, ON, Canada.

[3]Department of Otolaryngology, Kobe City Medical Center General Hospital, Kobe, Japan.

Corresponding Author's name: Norio Yamamoto

Affiliation: Department of Otolaryngology, Kobe City Medical Center General Hospital

E-mail:2-1-1 Minatojimaminami-cho, Chuo-ku, Kobe, 650-0047, Japan

E-mail address: yamamoto@ent.kuhp.kyoto-u.ac.jp

Conflicts of Interest: The authors declare that they have no conflicts of interest.

Abstract

Early B-cell factor 1 (EBF1) is a basic helix-loop-helix transcription factor essential for the differentiation of various tissues. Our single-cell RNA sequencing data suggest that *Ebf1* is expressed in the sensory epithelium of the inner ear. Here, we found that the *Ebf1* gene and its protein are expressed in the prosensory domain of the inner ear, medial region of the cochlear floor, inner ear mesenchyme, and cochleo-vestibular ganglion. *Ebf1* deletion results in incomplete formation of the spiral limbus and scala tympani, increased number of cells in the organ of Corti and Kölliker's organ, and aberrant course of the spiral ganglion axons. The inner ear-specific deletion of *Ebf1* revealed that scala tympani formation depended on *Ebf1* expressed in the otic mesenchyme. *Ebf1* deletion in the cochlear epithelia caused the proliferation of SOX2-positive cochlear cells at E13.5, indicating that EBF1 suppresses the proliferation of the prosensory domain and cells of Kölliker's organ to facilitate the development of appropriate numbers of hair and supporting cells. Furthermore, mice with deletion of cochlear epithelium-specific *Ebf1* showed poor postnatal hearing function. Our results suggest that *Ebf1* is essential for normal auditory function in mammals.

Introduction

The inner ear is a unique and complex organ that consists of bony and membranous labyrinths. The membranous labyrinth contains multiple sensory organs, including the cochlea, which is responsible for hearing and comprises three compartments (scalae): the scala vestibuli, scala tympani, and scala media. The scala vestibuli and scala tympani develop from the mesenchyme surrounding the inner ear (Sher, 1971). The scala media is situated between the scala vestibuli and scala tympani, which are separated from the scala media by the tectorial and basilar

membranes, respectively. Moreover, the scala media contains sensory epithelia that transduce sound into electrical signals via specialized sensory cells known as hair cells. Cochlear hair cells are located within the organ of Corti in the middle part of the scala media epithelium, and consist of one row of inner hair cells and three rows of outer hair cells. These hair cells are surrounded by at least seven types of non-sensory supporting cells: inner boundary cells, inner phalangeal cells, Deiters' cells, inner and outer pillar cells, Hensen's cells, and Claudius cells. The precise number and placement of mechanosensory hair cells and non-sensory supporting cells enable the accurate reception of mechanical stimulation of sound or body motion and its conversion into neural signals.

Inner ear development in mice begins with the formation of an ectodermal thickening called the otic placode, which is located adjacent to the hindbrain (Wu and Kelley, 2012). The otic placode invaginates to form a spherical structure called an otocyst at approximately embryonic day (E) 9.5. The ventral side of the otocyst forms the future sensory epithelium, where the sex-determining region Y-box transcription factor 2 (*Sox2*) is expressed (Kiernan et al., 2005). At E10.5, the cochlear and endolymphatic ducts and semicircular canals begin to form on the ventral and dorsal sides of the otocyst, respectively. After ventral cochlear duct formation becomes evident at E11, the ventral side of the cochlear duct (cochlear duct floor) begins to develop into a future sensory domain by expressing *Sox2* and *Jagged1* at E11.5 (Wu and Kelley, 2012). The *Sox2*-positive region becomes limited to the middle part of the ventral cochlear duct and is recognized as a prosensory domain at E13.5 and E14.5 (Kiernan et al., 2005; Ohyama et al., 2010). This region is located between two molecularly distinct nonsensory areas. The region medial to the prosensory domain toward the axis of the cochlea (modiolus) is called the greater epithelial ridge (GER) and transiently contains Kölliker's organ, which is composed of columnar

68 supporting cells during the developmental stage and becomes the inner sulcus with cuboidal cells
69 and the spiral limbus with interdental cells in the mature cochlea (Dayaratne et al., 2014).
70 Additionally, the GER is a source of sensory epithelia and has the potential to produce sensory
71 cells after the establishment of hair cells (Kubota et al., 2021).
72 The complex cellular structure and developmental processes of the inner ear depend on the
73 highly regulated expression patterns of signaling molecules and transcription factors. However,
74 the mechanisms underlying inner ear development are not fully understood. To comprehensively
75 elucidate these mechanisms, we analyzed the single-cell RNA-seq data of the inner ear epithelial
76 cells. In this study, we found that the early B-cell factor 1 gene (*Ebf1*) was upregulated in
77 clusters of sensory epithelial progenitors in the cochlea, macula, and crista, and confirmed that it
78 was expressed on the medial side of the cochlear duct floor, the prosensory area of the macula
79 and crista, and the spiral ganglion (Yamamoto et al., 2021).
80 EBF1 belongs to the EBF family of transcription factors and encodes four paralogous genes in
81 mammals, including mice and humans (Liberg et al., 2002). EBF family proteins comprise a
82 functional DNA-binding domain, transcription factor immunoglobulin, helix-loop-helix (HLH)
83 domain, and transactivation domain (Hagman et al., 1995), which are the characteristics of basic
84 HLH (bHLH) transcription factors. Similar to other bHLH transcription factors, EBF1 is
85 involved in various developmental processes, including the determination of cell fate and
86 differentiation of B lymphocytes and olfactory epithelia (Liberg et al., 2002).
87 Considering the various roles of EBF1 as a bHLH transcription factor, the importance of bHLH
88 transcription factors—such as ATOH1—in inner ear development, and the results of our
89 previous study confirming *Ebf1* expression in the inner ear sensory epithelium, we analyzed the
90 function of EBF1 in inner ear development. In the present study, we confirmed the

spatiotemporal expression of *Ebf1* during inner ear development and examined the effects of *Ebf1* deletion on inner ear development and hearing.

Results

Ebf1 is expressed in developing mouse cochlea

In silico analysis of embryonic inner ear epithelia suggested that *Ebf1* is predominantly expressed in the inner ear sensory epithelium during early development (Yamamoto et al., 2021). To quantify *Ebf1* expression at each stage of inner ear development, we performed quantitative reverse transcription polymerase chain reaction (qRT-PCR) using whole embryonic inner ears from E9.5 to P0 (Fig. 1A). The expression of *Ebf1* mRNA transcripts began to increase at E10.5 and reached a maximum at E13.5 (Fig. 1A). The relative expression level at E13.5 was approximately 10-fold higher than that at E9.5. The expression level then decreased but remained 7.5 times higher than that at E9.5 even at P0.

To describe the spatiotemporal expression patterns of *Ebf1* during inner ear development, we performed *in situ* hybridization (ISH) and immunohistochemistry (IHC) analyses on sections of the developing inner ear of wild-type mice from E9.5 to P0 (Fig. 1 B–D, Supplemental Fig. S1). We stained *Sox2*, which is expressed in the sensory progenitor region of the inner ear from the early developmental stages (Kiernan et al., 2005), as well as *Ebf1* on adjacent sections to specify the location of *Ebf1* expression, and compared the expression of the two genes and their products. First, we examined *Ebf1* expression at E13.5 (Fig. 1B), which is when the sensory epithelium of the inner ear forms and *Ebf1* expression level is maximized during inner ear development (Fig. 1A). *Ebf1* was expressed on the medial side of the cochlear floor, including the prosensory domain (white arrows in Fig. 1B), spiral ganglion (white asterisks in Fig. 1B), otic mesenchyme

(black asterisks in Fig. 1B), and parts of the prosensory regions of the vestibule and crista (black arrows in Fig. 1B). Compared with *Sox2*, *Ebf1* was expressed more medially within the cochlear floor, which developed into Kölliker's organ and the organ of Corti, and its expression in the vestibule was more restricted (Fig. 1B).

Subsequently, we examined the spatiotemporal expression of *Ebf1* throughout inner ear development, including the onset of expression in the inner ear epithelium, using inner ear sections from E9.5 to P0 (Fig. 1C, Supplemental Fig. S1). At E9.5, *Ebf1* was not expressed in the otocyst but was expressed in the progenitor cells of the cochleo-vestibular ganglion (CVG) (data not shown), which delaminate from the ventral side of the otocyst into the otic mesenchyme (Wu and Kelley, 2012). At E10.5, *Ebf1* expression was observed on the ventromedial side of the otocyst, which develops into the cochlear duct, and in the ventrolateral epithelium of the otocyst, which develops into the crista (black arrowheads in Fig. 1C). Additionally, *Ebf1* expression was detected in the otic mesenchyme (black asterisk in Fig. 1C) and CVG (white asterisk in Fig. 1C), which persisted until later stages (Supplemental Fig. S1). *Ebf1* was expressed in the border region, where the cochlear duct begins to elongate, at E11.5, in the medial side of the cochlear floor at E12.5, and in the future crista region in the vestibule at E11.5 and 12.5 (Supplemental Fig. S1). In the cochlea at E16.5 and E18.5, *Ebf1* was expressed throughout the organ of Corti and Kölliker's organ, whereas *Sox2* was expressed in the organ of Corti and the lateral half of Kölliker's organ (Fig. 1C and Supplemental Fig. S1), consistent with a previous report (Urness et al., 2015). *Ebf1* was expressed in the spiral ligaments, tympanic border cells (white arrowheads in Fig. 1C) (Taniguchi et al., 2012), vestibules, and crista (Fig. 1C). *Ebf1* expression was maintained until P0 (Supplemental Fig. S1).

IHC analysis showed that EBF1 was expressed throughout Kölliker's organ and the prosensory domain, whereas SOX2 was expressed in a part of Kölliker's organ and the prosensory domain (upper panels of Fig. 1D), which is consistent with the ISH results. The disappearance of the EBF1 signal from the cochlear epithelia and mesenchyme in conventional *Ebf1* knockout (*Ebf1*$^{-/-}$) mice confirmed the specificity of the anti-EBF1 antibody used in this study (Fig. 1D).

Ebf1 deletion altered the structure of the cochlear duct

Our ISH and IHC analyses, which showed the expression of *Ebf1* and its protein in both the developing inner ear epithelia and mesenchyme, suggest that *Ebf1* is involved in the development of both the inner ear sensory epithelium and otic mesenchyme. We used two mutant mouse strains to examine the roles of *Ebf1* in developing inner ears: an *Ebf1* conventional knockout (*Ebf1*$^{-/-}$) mouse (Lin and Grosschedl, 1995) and a Foxg1-Cre-mediated inner ear epithelia-specific conditional knockout mouse (*Foxg1Cre;Ebf1*$^{fl/fl}$) (Hébert and McConnell, 2000; Gyory et al., 2012) in which *Ebf1* expression remains localized in the inner ear mesenchyme.

Comparison of the gross morphology of the membranous labyrinth of the inner ear at E18.5 revealed no difference between *Ebf1*$^{+/+}$ and *Ebf1*$^{+/-}$ mice (Fig. 2A). However, after removing the lateral wall and roof of the cochlea to expose the cochlear floor, we found that *Ebf1*$^{-/-}$ mice had fewer turns in the cochlear duct than *Ebf1*$^{+/+}$ mice (white arrowhead in Fig. 2B).

Hematoxylin-eosin (HE) staining of the cochlea at E18.5 revealed incomplete formation of the scala tympani, particularly in the middle and apical turns of the cochlea of *Ebf1*$^{-/-}$ mice compared with those of control mice (arrowheads in Fig. 2C). Moreover, *Ebf1*$^{-/-}$ mice lacked a spiral limbus (sl; Fig. 2C); a lower number of cochlear turns was also observed in the cochlear sections of

these mice (arrows in the upper right panels in Fig. 2C), supporting the gross morphological observations.

Ebf1 was expressed in the otic mesenchyme from early to later developmental stages. To elucidate whether the hypoplastic scala tympani, fewer cochlear turns, and lack of spiral limbus were caused by the *Ebf1*-deficient mesenchyme, we examined the cochlear morphology of *Foxg1Cre;Ebf1*$^{fl/fl}$ and *Foxg1Cre;Ebf1*$^{fl/+}$ mice via HE staining. In contrast to the hypoplastic scala tympani of *Ebf1*$^{-/-}$ mice, the scala tympani of *Foxg1Cre;Ebf1*$^{fl/fl}$ mice was completely formed throughout the cochlear turns (left panels of Fig. 2C). The number of cochlear turns in *Foxg1Cre;Ebf1*$^{fl/fl}$ mice was similar to that in the control mice (*Foxg1Cre;Ebf1*$^{fl/+}$ mice). However, *Foxg1Cre;Ebf1*$^{fl/fl}$ mice lacked a spiral limbus, as observed in *Ebf1*$^{-/-}$ mice (Fig. 2C). These results suggest that *Ebf1* controls scala tympani formation and the turning of the cochlear duct through the mesenchyme, and the lack of the spiral limbus in *Ebf1*-deficient mice is secondarily caused by EBF1 malfunction within the epithelia.

Ebf1 deletion caused an increase in the number of cochlear hair, supporting, and Kölliker's organ cells

Observation of the cochlear epithelia in HE-stained samples revealed that both *Ebf1*$^{-/-}$ and *Foxg1Cre;Ebf1*$^{fl/fl}$ mice had deformed Kölliker's organs and organs of Corti (Ko and oC in Fig. 2C). To examine these phenotypes more comprehensively, we performed IHC analysis on inner ear sections and cochlear whole-mount samples from E18.5 (Fig. 3 and Supplemental Figs. S2 and S3).

IHC analysis of cochlear sections showed that *Ebf1* deletion increased the number of MYO7A-positive hair cells as well as SOX2-positive supporting and Kölliker's organ cells from the basal

182 to the apical region at E18.5 (Fig. 3A). An increase in the number of SOX2-positive cells within
183 the medial region of the cochlear floor was also observed at E14.5 (arrowhead in Fig. 1D). In
184 contrast, *Ebf1* deletion had no morphological effects on the vestibular sensory epithelium
185 (Supplemental Fig. S2). Additionally, the apical region of *Ebf1*$^{-/-}$ mouse cochleae contained
186 multiple layers of SOX2-positive cells (asterisk in Fig. 3A). IHC analysis of whole-mount
187 cochlear samples showed that *Ebf1*$^{-/-}$ mice had an increased number of MYO7A-positive hair
188 cells (Fig. 3B) and ectopic MYO7A-positive cells within the GER (arrows in Fig. 3B). Although
189 the normal cochlea has one and three rows of inner and outer hair cells, respectively, the mutant
190 cochlea had eight to nine rows of hair cells. We found ectopic hair cells in 7 of the 12 examined
191 cochleae. These ectopic MYO7A-positive cells contained stereocilia-like structures, as indicated
192 by phalloidin staining (arrows in Fig. 3C). Increased numbers of supporting cells were confirmed
193 in whole-mount cochlear samples by IHC staining of SOX2 (Fig. 3D), a supporting and
194 Kölliker's organ cell marker, and PROX1 (Fig. 3E), a pillar and Deiters' cell marker
195 (Bermingham-McDonogh et al., 2006).
196 To quantify the number of hair and supporting cells, we counted the cells in three regions within
197 the cochlea (basal, middle, and apical regions; Fig. 4A) and measured the number of MYO7A- or
198 PROX1-positive cells per 200 μm at E18.5. For SOX2-positive cells, we counted the cell number
199 per 100 μm only in the basal regions at E18.5. The results showed that the cochlear hair cell
200 number was significantly increased in *Ebf1*$^{-/-}$ mice compared to *Ebf1*$^{+/+}$ mice in all three regions
201 (Fig. 4B). *Ebf1*$^{+/-}$ mice exhibited a significantly higher number of cochlear hair cells than *Ebf1*$^{+/+}$
202 mice in the middle and apical regions (Fig. 4B, $p < 0.0001$). The hair cell numbers per 200 μm of
203 *Ebf1*$^{+/+}$, *Ebf1*$^{+/-}$, and *Ebf1*$^{-/-}$ mice were 142.3 ± 9.0, 150.0 ± 2.8, and 367.5 ± 30.8 in the basal

204 regions; 152.8 ± 8.1, 190.3 ± 7.0, and 363.0 ± 22.4 in the middle regions; and 154.5 ± 5.1, 183.5
205 ± 6.8, and 440.3 ± 23.8 in the apical regions, respectively.
206 SOX2-positive cells, constituting a part of Kölliker's organ cells and supporting cells within
207 organs of Corti, also increased in number by 1.7 times in *Ebf1*$^{-/-}$ mice compared to *Ebf1*$^{+/+}$ mice
208 (Fig. 4C). PROX1-positive cell numbers significantly increased in *Ebf1*$^{-/-}$ mice compared to
209 *Ebf1*$^{+/+}$ mice only in the basal and middle regions (Fig. 4D). In the apical region, the number of
210 PROX1-positive cells was similar to that in *Ebf1*$^{-/-}$ and *Ebf1*$^{+/+}$ mice. The numbers of PROX1-
211 positive cells in *Ebf1*$^{+/+}$ and *Ebf1*$^{-/-}$ mice were 203.3 ± 2.2 and 439.0 ± 15.4, 228.0 ± 16.8 and
212 389.8 ± 10.4, and 196.0 ± 27.3 and 204.5 ± 19.6 in the basal, middle, and apical regions,
213 respectively.
214 We performed IHC analysis using more specific markers to reveal which population of hair or
215 supporting cells increased in number in *Ebf1*$^{-/-}$ mice (Supplemental Fig. S3). We immunostained
216 whole-mounted cochlea at E18.5 with anti-VGLUT3 and anti-p75 antibodies, which indicate
217 inner hair (Li et al., 2018) and pillar cells (von Bartheld et al., 1991), respectively. VGLUT3-
218 positive inner hair cells, which are arranged in a single row in wild-type mice, were found to be
219 increased in number in *Ebf1*$^{-/-}$ mice (Supplemental Fig. S3A), indicating an increase in both inner
220 and outer hair cells. The number of p75-positive pillar cells, which separate inner and outer hair
221 cells, did not increase in *Ebf1*$^{-/-}$ mice (Supplemental Fig. S3B). Considering that PROX1-positive
222 cells indicate pillar and Deiters' cells, the number of Deiters' cells increased in *Ebf1*$^{-/-}$ mice.
223 However, the arrangement of pillar cells was disrupted in *Ebf1*$^{-/-}$ mice (arrows in Supplemental
224 Fig. S3B), which was reflected in the appearance of VGLUT3 cells in the outer hair cell region
225 of *Ebf1*$^{-/-}$ mice (arrowheads in Supplemental Fig. S3A).

The total cochlear length, measured based on the length of the MYO7A-positive region (Supplemental Fig. S4A), was slightly, but significantly, shorter in *Ebf1*$^{-/-}$ mice than in *Ebf1*$^{+/+}$ and *Ebf1*$^{+/-}$ mice (Supplemental Fig. S4B, $p < 0.001$).

Ebf1 deletion caused the aberrant spiral ganglion and nerve fibers

As *Ebf1* is expressed in the spiral ganglion and the number of hair cells, a target of the spiral ganglion cell axon, increased in *Ebf1*$^{-/-}$ mice, we examined the spiral ganglion morphology and innervation of cochlear hair cells with IHC using anti-Tubulin β 3 (TUJ1) antibodies at E18.5 (Supplemental Fig. S5).

Compared with *Ebf1*$^{+/+}$ mice, which exhibited axons extending from the spiral ganglion cells to the cochlear hair cells, *Ebf1*$^{-/-}$ mice had spiral ganglion cells (sg in Supplemental Fig. S5A) under the organs of Corti (arrows in Supplemental Fig. S5A), as well as in their normal position. The axons, which usually run parallel to the rows of outer hair cells, formed a reticulation within the *Ebf1*$^{-/-}$ mouse cochlear hair cell regions (Supplemental Fig. S5B). Moreover, the innervation reached Kölliker's organ (arrowheads and brackets in Supplemental Fig. S5A) as well as the organ of Corti.

Ebf1 deletion changed the distribution of JAG1-positive Kölliker's organ cells, the differentiation timing of a prosensory domain, and the proliferation of SOX2-positive cells

As *Ebf1*$^{-/-}$ mice had increased numbers of cochlear hair cells, which were differentiated from the prosensory domain, we investigated its specification, differentiation, proliferation, and cell death in the *Ebf1*$^{-/-}$ mouse cochlear duct floor.

First, to determine whether formation of the prosensory domain was affected by *Ebf1* deletion, we examined the formation of regions medial and lateral to the prosensory domain. Because these regions express FGF10 and BMP4 to induce non-sensory or sensory epithelia in the cochlear floor (Ohyama et al., 2010; Urness et al., 2015), respectively, we performed ISH for *Fgf10* and *Bmp4* in the basal region of the cochlear duct of *Ebf1*$^{+/+}$ *and Ebf1*$^{-/-}$ mice at E13.5 (Fig. 5A). The formation of both regions was similar in *Ebf1*$^{+/+}$ and *Ebf1*$^{-/-}$ mice, suggesting that *Ebf1* is not involved in the development of cell populations expressing *Fgf10* or *Bmp4*. To verify the medial cell population more precisely, we immunostained E13.5 and E14.5 cochleae with an anti-JAG1 antibody (Fig. 5A), as JAG1 is exclusively expressed in Kölliker's organ, a part of the medial region, at this stage (Ohyama et al., 2010). JAG1-positive cells in *Ebf1*$^{-/-}$ mouse cochlea expanded to the more medial region compared with those in *Ebf1*$^{+/+}$ mouse cochlea at E13.5 and E14.5 (arrowheads in Fig. 5A).

Subsequently, we examined the expression of *Atoh1* within the prosensory domain via ISH at E14.5 and E15.5 (Fig. 5B), as *Atoh1* is necessary for hair cells to differentiate from the prosensory cell population (Bermingham et al., 1999) and its expression indicates the initiation of hair cell development from the prosensory domain. Compared to *Ebf1*$^{+/+}$ mice that expressed *Atoh1* within the prosensory domain from E14.5, *Atoh1* mRNA was not detected in the basal to middle region of the E14.5 *Ebf1*$^{-/-}$ mouse cochlea, although the vestibular organs expressed *Atoh1* within the prosensory epithelia. However, E15.5 *Ebf1*$^{-/-}$ mice exhibited an *Atoh1* signal within the prosensory domain of the cochlea. This result suggests that while the cell fate specification of sensory epithelia in the cochlea is not affected, its timing is delayed by *Ebf1* deletion. Considering that the differentiation of cochlear sensory epithelia promotes the transition from the basal to apical turns of the cochlea (Sher, 1971), the expression of hair and supporting

271 cell markers at a later stage, E18.5, also indicated delayed differentiation of *Ebf1*$^{-/-}$ mouse
272 cochleae (Supplemental Fig. S3). These markers were found to be detected in more basal
273 cochlear regions in *Ebf1*$^{-/-}$ mice than in *Ebf1*$^{+/+}$ mice.
274 The expansion of the JAG1-positive cell area and the increased numbers of hair and supporting
275 cells suggest that the enhancement of proliferation or suppression of cell death occurs within the
276 prosensory domain and Kölliker's organ of *Ebf1*$^{-/-}$ mouse cochlea. To identify the mechanisms
277 that correlate with the functions of EBF1 within the cochlea, we tested the proliferation and
278 apoptotic status of *Ebf1*$^{-/-}$ mouse cochlea. To evaluate the proliferation status of the prosensory
279 domain and Kölliker's organ, we immunostained cochlear sections with SOX2, a marker of the
280 prosensory domain and a part of Kölliker's organ, and 5-ethynyl-2′-deoxyuridine (EdU) at E12.5,
281 13.5, 14.5, and 16.5 after administering EdU to pregnant mice (Fig. 6A). Quantification of
282 SOX2-positive cells showed that their number decreased in *Ebf1*$^{+/+}$ mice from E12.5 onward
283 (Fig. 6B), and their location was limited to the prosensory domain (brackets in Fig. 6A). In
284 contrast, SOX2-positive cells in *Ebf1*$^{-/-}$ mouse cochlea were found both in the prosensory domain
285 and the medial region, even at E13.5, which was consistent with the results of JAG1
286 immunostaining (Fig. 5A). The number of SOX2-positive cells in *Ebf1*$^{-/-}$ mice was similar to that
287 in *Ebf1*$^{+/+}$ mice at E12.5, but increased at E13.5 and returned to the E12.5 level at E14.5.
288 Therefore, the number of SOX2-positive cells in *Ebf1*$^{-/-}$ mice was significantly higher than those
289 in *Ebf1*$^{+/+}$ mice at E13.5 and E14.5 (Fig. 6B). The number of EdU-positive proliferating cells
290 within SOX2-positive cells was significantly higher in *Ebf1*$^{-/-}$ mice than in *Ebf1*$^{+/+}$ mice at E13.5
291 and E14.5 (Fig. 6C). As the number of SOX2-positive cells increased in *Ebf1*$^{-/-}$ mice after E13.5
292 (Fig. 6B), normalization of SOX2-positive cell numbers was necessary to correctly evaluate the
293 proliferation status of SOX2-positive cells. We calculated the proportion of EdU-positive cells

among SOX2-positive cells and found that the proliferation was enhanced in the SOX2-positive cells of *Ebf1*$^{-/-}$ mouse cochlea only at E13.5 (49.8 ± 4.3%) compared with that in *Ebf1*$^{+/+}$ mouse cochlea (37.8 ± 4.2%) (Fig. 6D). These results suggested that EBF1 suppressed the proliferation of SOX2-positive cells within a limited time window. Morphologically, a difference in proliferation was observed in the prosensory domain, as indicated by EdU immunostaining (brackets at E13.5; Fig. 6A). EdU staining was observed in the Kölliker's organs of *Ebf1*$^{-/-}$ mice, even at E16.5, but not observed in *Ebf1*$^{+/+}$ mice (E16.5 of Fig. 6A).

The loss of proliferation within the prosensory domain around E13.5 (bracket in the *Ebf1*$^{+/+}$ sample at E13.5, Fig. 6A) has been well documented in previous studies (Chen and Segil, 1999; Chen et al., 2002). The post-mitotic domain is called the zone of non-proliferating cells (ZNPC), and is characterized by the expression of the cyclin-dependent kinase inhibitor p27Kip1. To confirm the EdU immunostaining results, we performed p27Kip1 immunostaining at E13.5 and E14.5 (Fig. 6E). Although p27Kip1 was detected in the prosensory domain of *Ebf1*$^{+/+}$ mice at E13.5, it was not expressed in *Ebf1*$^{-/-}$ mouse cochlea at this stage (arrows in Fig. 6E), which was consistent with the results of EdU detection. At E14.5, p27Kip1 was detected in a larger area of the middle part of *Ebf1*$^{-/-}$ mouse cochlear floors than in those of *Ebf1*$^{+/+}$ mice.

In contrast, apoptosis within the inner ear or cochlear duct did not increase in *Ebf1*$^{-/-}$ mice at E11.5 and E13.5, compared with that in *Ebf1*$^{+/+}$ mice (Supplemental Fig. S6).

Ebf1 deletion impairs auditory function

The aberrant cochlear sensory epithelia observed in *Ebf1*-deleted mice suggest that hearing ability is impaired in these mice. To evaluate the effect of *Ebf1* deletion on auditory function, we measured the auditory brainstem response (ABR) (Fig. 7A) and distortion product of otoacoustic

emissions (DPOAE) (Fig. 7B) in P21 *Foxg1Cre;Ebf1*$^{fl/fl}$ mice. We did not use *Ebf1*$^{-/-}$ mice for this analysis to avoid embryonic lethality and to eliminate the effects of the hypoplastic scala tympani observed in *Ebf1*$^{-/-}$mice on auditory function. The phenotype of *Foxg1Cre;Ebf1*$^{fl/fl}$ mice was evaluated using whole-mount cochlear samples collected at P23 (Fig. 7C). We observed a marked increase in the number of cochlear hair cells in *Foxg1Cre;Ebf1*$^{fl/fl}$ mice, comparable to the morphology of E18.5 *Ebf1*$^{-/-}$ mice (Fig. 3B and Fig. 7C).

ABR measurement showed significant elevations of thresholds of the response to sound in *Foxg1Cre;Ebf1*$^{fl/fl}$ mice at all frequencies examined (10 kHz, 93.3 ± 2.5 dB; 20 kHz, 86.7 ± 3.8 dB; 40 kHz, 105.0 ± 0.0 dB) (Fig. 7A) compared with control mice, indicating severe hearing loss in *Ebf1*-deleted mice. Subsequently, we performed DPOAE tests to assess the function of the increased number of outer hair cells caused by *Ebf1* deletion because DPOAE detects nonlinear responses of outer hair cells to sound. The DPOAE responses in *Foxg1Cre;Ebf1*$^{fl/fl}$ mice were significantly lower than those in control mice (Fig. 7B). The decreased DPOAE response in *Foxg1Cre;Ebf1*$^{fl/fl}$ mice also suggests that the increased number of hair cells caused by *Ebf1* deletion did not function as outer hair cells.

Discussion

The results of this study indicate a novel and interesting role of *Ebf1* in the development of the cochlear epithelia and otic mesenchyme. *Ebf1* is involved in the formation of appropriate numbers of hair and supporting cells within the cochlear sensory epithelia. Moreover, *Ebf1* is important for the development of the scala tympani, which is formed through *Ebf1* expression within the mesenchyme, and spiral ganglion cells. The *Ebf1* deficiency in the cochlear epithelia resulted in impaired auditory function, suggesting that *Ebf1* is necessary for normal auditory

340 function.

341 Since EBF1 was originally identified from the regulators of early B cell differentiation (Hagman
342 et al., 1991) and olfactory-specific genes (Wang and Reed, 1993), the expression patterns and
343 functions of EBF1 have been studied in B lymphocytes (Lin and Grosschedl, 1995), olfactory
344 epithelia (Wang et al., 1997), striatum neurons (Garel et al., 1999), the retina (Jin et al., 2010; Jin
345 and Xiang, 2011), the kidney (Fretz et al., 2014; Nelson et al., 2019), bone marrow stromal cells
346 (Derecka et al., 2020), osteoblasts (Hesslein et al., 2009), and adipose tissue (Jimenez et al.,
347 2007). The expression of *Ebf1* and its protein product has been reported in all three germinal
348 layers, and the function of EBF1 varies (Liberg et al., 2002). EBF1 is involved in cell fate
349 specification (Jin et al., 2010; Nechanitzky et al., 2013), cell differentiation (Lin and Grosschedl,
350 1995; Wang et al., 1997; Garel et al., 1999; Jimenez et al., 2007; Jin and Xiang, 2011; Nieminen-
351 Pihala et al., 2021), cell maturation (Fretz et al., 2014; Nelson et al., 2019), cell migration
352 (Derecka et al., 2020), and path finding by neurons (Garel et al., 2000; Jin and Xiang, 2011),
353 mainly during the developmental stage in mammals.

354 The present study revealed that *Ebf1* is expressed not only in the inner ear epithelium and spiral
355 ganglion but also in the otic mesenchyme. As the inner ear epithelium and spiral ganglion cells
356 are derived from the ectoderm (Wu and Kelley, 2012), *Ebf1* is expressed in both ectodermal and
357 mesenchymal tissues within the inner ear. Its expression in the inner ear began at approximately
358 E10.5, as confirmed by qRT-PCR and ISH (Fig. 1A and C). Within the inner ear epithelia, *Ebf1*
359 showed different expression patterns in the cochlear and vestibular organs from E13.5 to E18.5.
360 In the vestibule and crista, *Ebf1* was expressed in parts of *Sox2*-positive prosensory regions (Fig.
361 1B, black arrows and C). However, its expression in the cochlea was not limited to a part of the
362 *Sox2*-positive prosensory domain (white arrows in Fig. 1B) but expanded toward a more medial

363 region in the cochlear floor, where Kölliker's organ exists (Fig. 1B–D). Thus, the *Ebf1*
364 expression area comprised most of the GER. This difference suggests distinct functions of *Ebf1*
365 in the development of cochlear and vestibular organs.
366 To elucidate the function of *Ebf1* in inner ear development, we examined the inner ear
367 morphology of *Ebf1* conventional and inner ear-specific conditional knockout mice. As
368 suggested by the expression study, the cochlear and vestibular organs exhibited different
369 morphological phenotypes. No differences were observed in the vestibular morphology of
370 *Ebf1*$^{+/+}$ and *Ebf1*$^{-/-}$ mice (Supplemental Fig. S2), despite *Ebf1* expression. As observed in the
371 olfactory epithelia and retina (Wang and Reed, 1993; Wang et al., 1997; Jin et al., 2010), the
372 deletion of *Ebf1* may be compensated for by other *Ebf* family genes, and studies in other mutant
373 mice, including double- or triple-knockout mice and mice with the dominant negative form of
374 the EBF protein, are needed to elucidate the function of EBF1 in the vestibular organ.
375 In contrast, the cochlea of *Ebf1*-deleted mice showed various phenotypes, indicating that other
376 *Ebf* subtypes do not have redundant functions with *Ebf1* in the cochlea as in B cells, osteoblasts,
377 and the striatum (Lin and Grosschedl, 1995; Garel et al., 1999; Nieminen-Pihala et al., 2021). HE
378 staining revealed loss of the scala tympani and spiral limbus (Fig. 2C). Because both structures
379 are derived from mesenchymal tissues (Sher, 1971; Phippard et al., 1999), we hypothesized that
380 these phenotypes reflect the roles of EBF1 in cochlear mesenchymal tissue. To confirm this, we
381 compared the formation of the scala tympani and spiral limbus in two *Ebf1*-deleted mouse strains,
382 conventional (*Ebf1*$^{-/-}$ mice) and epithelia-specific conditional (*Foxg1Cre;Ebf1*$^{fl/fl}$ mice) *Ebf1*
383 knockout mice (Fig. 2C). Although the scala tympani developed normally in *Foxg1Cre;Ebf1*$^{fl/fl}$
384 mice, the spiral limbus was hypoplastic in both *Foxg1Cre;Ebf1*$^{fl/fl}$ and *Ebf1*$^{-/-}$ mice. These results
385 clearly indicate that EBF1 in the cochlear mesenchyme is involved in the formation of the scala

386 tympani. In contrast, spiral limbus formation depends on both mesenchymal and epithelial or
387 epithelial expression of *Ebf1*. Because *Ebf1* was expressed in both the epithelia and mesenchyme
388 (Fig. 1B and Supplemental Fig. S1), we were unable to determine which was the case in this
389 study; however, mesenchyme-specific deletion of *Ebf1* will confirm the tissue responsible for
390 inducing the spiral limbus. Gross morphological observation (Fig 2B) and MYO7A staining of
391 the whole-mount cochlea (Supplemental Fig. S4) showed that the length of the cochlear duct was
392 shorter in *Ebf1*$^{-/-}$ mice. As the number of cochlear turns in the cochlear section was lower in
393 *Ebf1*$^{-/-}$ mice than in *Foxg1Cre;Ebf1*$^{fl/fl}$ mice, this phenotype reflects the function of mesenchymal
394 EBF1 in regulating the length of the cochlear duct.
395 In addition to the mesenchyme, more prominent roles of *Ebf1* have been found in the cochlear
396 epithelia. In both *Ebf1*$^{-/-}$ and *Foxg1Cre;Ebf1*$^{fl/fl}$ mice, the numbers of both hair and supporting
397 cells increased throughout cochlear turns at E18.5 (Fig. 3 and 4). We observed an increase in the
398 numbers of both inner and outer hair cells (Supplemental Fig. S3A). However, more detailed
399 IHC analysis of supporting cells showed that only the Deiters' cells increased in number among
400 PROX1-positive and SOX2-positive cells located medial to the organs of Corti, and the number
401 of pillar cells did not increase (Supplemental Fig. S3B). This phenotype suggests that EBF1 is
402 involved in the regulation of hair and supporting cell number during cochlear development. To
403 determine the mechanisms of hair and supporting cell number increase under *Ebf1* knockout
404 conditions, we evaluated the specifications and differentiation of the cochlear prosensory domain
405 and its proliferation and cell death status. We found that the formation of cochlear non-sensory
406 regions medial and lateral to the prosensory domain were normal in *Ebf1*$^{-/-}$ mice (Fig. 5A).
407 Although the lateral region marker BMP4 has been reported to affect the development of the
408 prosensory domain (Ohyama et al., 2010), the normal formation of this region indicates that the

409 phenotypes of *Ebf1*$^{-/-}$ mouse cochlear sensory epithelia were not caused by aberrant BMP4
410 expression, but by factors within the prosensory domain. In contrast to markers outside the
411 prosensory domain, the molecules expressed in the prosensory domain and Kölliker's organs,
412 JAG1 and SOX2, showed abnormal expression patterns (Fig. 1D, Fig. 3A, and Fig. 5A). These
413 two molecules were expressed in a more medial region of the *Ebf1*$^{-/-}$ mouse cochlear floor at
414 E14.5 and E18.5. The fact that EBF1 was expressed in a more medial region than SOX2 in wild-
415 type mice indicates that it plays a role in suppressing the localization of JAG1- and SOX2-
416 positive cells in the most medial region. The study of proliferation status within the SOX2-
417 positive cells showed that *Ebf1* deletion enhanced the proliferation of SOX2-positive cells
418 specifically at E13.5 (Fig. 6 D), which was supported by the loss of p27Kip1 expression in the
419 possible prosensory domain of the *Ebf1*$^{-/-}$ mice at E13.5 (Fig. 6E). The highest *Ebf1* expression
420 level at E13.5 (Fig. 1A) may be related to these phenotypes in *Ebf1*$^{-/-}$ mice. This aberrant
421 proliferation within SOX2-positive cells was suggested to increase the numbers of hair and
422 supporting cells at later stages (Fig. 3A, B, D, and E). Evaluation of hearing ability at the
423 postnatal stage showed that an increase in hair and supporting cell numbers resulted in an
424 increased hearing threshold (Fig. 7). These results indicate that EBF1 suppresses the proliferation
425 of SOX2-positive cells and thus contributes to the development of appropriate numbers of hair
426 and supporting cells, resulting in the development of normal auditory function. Because the
427 SOX2-positive cells within the E13–14 cochlea become Kölliker's organ as well as lateral and
428 medial prosensory domains at a later stage (Kolla et al., 2020) and the GER has the potential to
429 form cochlear sensory epithelia (Kubota et al., 2021), EBF1 expressed in SOX2-positive cells
430 regulates the number of hair and supporting cells. Several lines of evidence support the function
431 of EBF1 to suppress cell proliferation. Human EBF1 has been reported to suppress the

proliferation of malignant tumors (Shen et al., 2020), and the deletion of *Rb1*, a known tumor suppressor and cell cycle regulator (Lipinski and Jacks, 1999; Classon and Harlow, 2002), results in the same morphology in the cochlea as that caused by *Ebf1* deletion (Sage et al., 2005).

The expression of mature cochlear cell markers, including MYO7A, VGULT3, and p75, in *Ebf1*$^{-/-}$ mice indicated that each cell type developed with normal cell fate specification. Although some GER cells in *Ebf1*$^{-/-}$ mice expressed the hair cell marker MYO7A (Fig. 3B and C) and cell fate specification appeared to deteriorate, the penetrance of this phenotype was low. Cell fate may be regulated by EBF1 in the cochlea to a small extent; however, cell specification does not play a prominent role in cochlear EBF1, which is different from other tissues, including B lymphocytes (Nechanitzky et al., 2013). In contrast, several results from our study indicate that the speed of differentiation appears to deteriorate in the *Ebf1*$^{-/-}$ mouse cochlea. The expression of *Atoh1* within the cochlear prosensory domain, which was observed at E13.5 in wild-type mice, was detected as late as E14.5 in *Ebf1*$^{-/-}$ mice (Fig. 5B). The regions where VGLUT3- and p75-positive cells were detected in *Ebf1*$^{-/-}$ mouse cochlea were more basal than those in *Ebf1*$^{+/+}$ mouse cochlea at E18.5 (Supplemental Fig. S3). This delay in differentiation may be caused by the aberrant proliferation of the prosensory domain in *Ebf1*$^{-/-}$ mice, as the deterioration of proliferation affects the differentiation of cells (Ruijtenberg and van den Heuvel, 2016).

In addition to the cochlear epithelia and mesenchyme, deletion of *Ebf1* resulted in an altered neuroaxonal composition of spiral ganglion neuronal cells in the organ of Corti, suggesting that EBF1 may also affect the pathfinding of spiral ganglion cells within the cochlea, as observed in the aberrant pathfinding of facial branchiomotor neurons and retina (Garel et al., 2000; Jin and Xiang, 2011). The present study was limited to IHC analysis of TUJ1, and further studies are needed to elucidate the role of *Ebf1* in spiral ganglion differentiation and development. Spiral

ganglion axons synapse with hair cells from within the otic mesenchyme, and axons extend through the mesenchyme to innervate the organ of Corti (Coate and Kelley, 2013). Thus, deletion of *Ebf1* in the mesenchyme may also contribute to the phenotype observed in the spiral ganglion cells.

The expression of *Ebf1* in the medial region of the cochlear floor (Fig. 1B, C, and D) and the spiral limbus loss (Fig. 2C) and ectopic MYO7A-positive cells within the GER (Fig. 3B and C) in *Ebf1*-deleted mice suggest that EBF1 has functions within the GER or Kölliker's organ. Recently, PRDM16 was reported to be a marker of Kölliker's organ and an important molecule in its development (Ebeid et al., 2022). *Prdm16* null mutant mice showed phenotypes similar to those of *Ebf1*-deleted mice, including shortened cochlear length, spiral limbus loss, and ectopic hair cells within the GER. Moreover, the *Prdm16* null mutant mouse cochlear duct expressed approximately half the amount of *Ebf1* compared to the wild-type mouse cochlear duct (Ebeid et al., 2022), suggesting that EBF1 is involved in the development of Kölliker's organ. However, if PRDM16 is the direct upstream regulator of EBF1, the *Ebf1* expression level should be much less in *Prdm16* null mutant mice, and these mice should exhibit increased hair and supporting cells and loss of scala tympani, as observed in *Ebf1*$^{-/-}$ mice. Thus, PRDM16 does not control the expression of EBF1.

The phenotypes of the increased numbers of hair and supporting cells suggest the involvement of previously reported molecules crucial for the development of cochlear sensory epithelia, including Notch signal-related molecules (Yamamoto et al., 2011) and SOX2 (Kiernan et al., 2005), in the regulation of *Ebf1* expression. However, *Foxg1Cre*-mediated *Notch 1*- or *Sox2*-deleted mice do not show lower *Ebf1* expression levels in striatal neurons (Mason et al., 2005; Ferri et al., 2013), suggesting that Notch signaling and SOX2 do not control EBF1 expression.

Identification of the molecules upstream and downstream of EBF1 will be the next step in revealing the precise function of EBF1 in the cochlea and the grand scheme of inner ear development.

In conclusion, our study confirms that *Ebf1* and its protein are expressed in the epithelia of the inner ear prosensory domain as well as in Kölliker's organ, the mesenchyme, and CVG cells within the cochlea, and play important roles in the formation of each structure. Epithelial EBF1 regulates the number of cochlear hair and supporting cells by suppressing the proliferation of the prosensory domain and Kölliker's organ cells, mainly at E13.5, whereas mesenchymal EBF1 contributes to scala tympani formation. Therefore, epithelial EBF1 is crucial for normal hearing in mammals.

Material and Methods

Animals

Slc: ICR mice were purchased from Japan SLC (Hamamatsu, Japan). *Ebf1*$^{-/-}$ mice (Lin and Grosschedl, 1995) and *Ebf1*$^{fl/fl}$ (Gyory et al., 2012) were used in this study. *Ebf1*$^{fl/+}$ mice were crossed with *Foxg1*$^{Cre/+}$ *mice* (*Foxg1Cre*) (Hébert and McConnell, 2000) and *Ebf1*$^{-/-}$ or *Foxg1Cre;Ebf1*$^{fl/fl}$ mice were used as experimental animals. Additionally, *Ebf1*$^{+/+}$, *Ebf1*$^{+/-}$, or *Foxg1Cre;Ebf1*$^{fl/+}$ mice were used as controls.

Ebf1$^{+/-}$, *Foxg1Cre*, and *Ebf1*$^{fl/fl}$ mice were maintained on a C57BL/6 background. All experimental protocols were approved by the Animal Research Committee of Kyoto University (Med Kyo 20132, Kyoto, Japan). All animal experiments were performed according to the National Institutes of Health Guidelines for the Care and Use of Laboratory Animals. All the animals used in this study were maintained at the Institute of Laboratory Animals, Graduate

School of Medicine, Kyoto University. The mice were mated in the evening, and vaginal plugs were checked early in the morning. The day a vaginal plug was detected was defined as E0.5.

qRT-PCR

Inner ears were dissected from E9.5, E10.5, E11.5, E12.5, E13.5, E14.5, E16.5, E18.5, and P0 ICR mice. After the surrounding tissue was removed from the inner ears, at least four samples were immersed in TRIzol Reagent (Thermo Fischer Scientific, Waltham, MA, USA) and preserved at −80 °C until RNA extraction. Total RNA was extracted using the RNeasy™ Mini Kit (QIAGEN, Venlo, Netherlands) and reverse transcribed using the ReverTra Ace™ qPCR RT Master Mix with gDNA Remover (TOYOBO, Osaka, Japan). The cDNA was mixed with PowerUp SYBR Green Master Mix (Applied Biosystems) and various sets of gene-specific forward and reverse primers and subsequently subjected to real-time PCR quantification using a StepOnePlus Real-Time PCR System (Applied Biosystems, Waltham, MA, USA). The following primer sequences were used: *Ebf1* forward, AACTCCAAGCACGGGCGGAG; *Ebf1* reverse, CGGGCTGATGGCTTTGATACAGG; *Rplp0* forward, CACTGGTCTAGGACCCGAGAAG; *Rplp0* reverse, GGTGCCTCTGGAGATTTTCG. Relative mRNA expression levels were calculated using the standard curve method, and the mouse housekeeping gene *Rplp0* was used as an invariant control.

ISH

Whole embryos (E9.5–E11.5) and whole heads (E12.5–P0) were fixed in 4% paraformaldehyde (PFA; Nacalai Tesque, Kyoto, Japan) in 0.1 M phosphate-buffered saline (PBS) at 4 °C overnight. Samples were cryoprotected in 30% sucrose/PBS (Nacalai Tesque), embedded in

Tissue-Tek® O.C.T.™ compound (Sakura Finetek Japan, Tokyo, Japan), and sectioned at 10-μm thickness using a cryostat (CryoStar™ NX70; Thermo Fisher Scientific). The sections were subsequently mounted on silane-coated glass slides (Matsunami Glass, Osaka, Japan).

cDNA fragments were generated by PCR using E13.5 inner ear cDNA of Slc:ICR mice and subsequently cloned into the pCR®-Blunt II-TOPO® vector (Invitrogen, Waltham, MA, USA) to prepare RNA probe templates. We synthesized digoxigenin (DIG)-labeled sense and antisense RNA probes using a DIG RNA Labeling Kit (Roche, Basel, Switzerland) after digestion with the appropriate restriction enzymes *Bam*HI-HF, *Hind*III, *Not*I-HF, *Sac*I, or *Xho*I (New England Biolabs, Ipswich, MA, USA). The following probes were used for ISH: *Ebf1* (NM_001,290,709, nucleotides 1436–2269), *Sox2* (IMAGE clone: 6413283), *Bmp4* (NM_007554.3, nucleotides 1013-1876), *Atoh1* (NM_007500.5, nucleotides 13-2111), and *Fgf10* (NM_008002.5, nucleotides 571-1027). Each corresponding sense probe was used as a negative control.

Sections were fixed with 4% PFA and 0.2% glutaraldehyde (Nacalai Tesque) in PBS at room temperature (RT) for 10 min, bleached with 6% hydrogen peroxidase (FUJIFILM Wako Pure Chemical Corporation, Osaka, Japan) in 0.1% Tween-20 in PBS (PBST) at RT for 10 min, treated with proteinase K (20 μg/μL, Roche) for 5 min, and re-fixed with 4% PFA and 0.2% glutaraldehyde in PBS at RT for 10 min.

The prehybridization was performed in hybridization solution containing 50% formamide (Nacalai Tesque), 5× saline sodium citrate buffer (SSC, Nacalai Tesque; adjusted to pH 4.5 with citrate), 1% sodium dodecyl sulfate (Sigma-Aldrich, St. Louis, MO, USA), 50 μg/mL yeast RNA (Invitrogen), and 50 μg/mL heparin (Sigma-Aldrich) at 70 °C for 1 h. For hybridization, we incubated the sections in a hybridization solution with a 0.2 μg/mL DIG-labelled RNA probe at 70 °C for 16 h in sealed plastic bags.

547 Sections were rinsed first in 50% formamide with 6× SSC and 1% sodium dodecyl sulfate at
548 70 ℃, then in 50% formamide with 2.4× SSC at 65 ℃, and finally in 1× Tris-buffered saline
549 (Nacalai Tesque) with 0.1% Tween 20 (TBST) at RT. Sections were blocked with 5% sheep
550 serum (Sigma-Aldrich) and incubated with a 1:4000 dilution of Anti-Digoxigenin-AP Fab
551 fragments (Roche) at 4 ℃ overnight.
552 After rinsing with TBST and NTMT containing 100 mM NaCl (Nacalai Tesque), 100 mM Tris-
553 HCl pH 9.5, 10 mM $MgCl_2$ (FUJIFILM Wako Pure Chemical Corporation), 0.1% Tween-20, and
554 480 μg/mL levamisole (Sigma-Aldrich), the sections were incubated with nitro-blue tetrazolium
555 chloride (Roche) and 5-bromo-4-chloro-3-indolyl phosphate solution (Roche). Images were
556 captured using a BX-50 microscope (Olympus Corp., Tokyo, Japan).
557
558 *IHC analysis*
559 IHC sections were prepared in a manner similar to that used for ISH.
560 After washing with PBS, all samples were incubated with Blocking One Histo (Nacalai Tesque)
561 for 10 min at RT and 10% normal donkey serum (Sigma-Aldrich) in PBS/0.5% Triton X- 100
562 with 5% Blocking One Histo for 30 min at RT.
563 The samples were stained with primary antibodies at 4 ℃ overnight or RT for 1 h. After washing
564 with PBST, the samples were incubated with Alexa Fluor secondary antibodies. F-actin (actin
565 filaments) was stained with phalloidin 647 (1:500; Thermo Fisher Scientific) at RT for 1 h.
566 Nuclei were stained with 4′,6-diamidino-2-phenylindole (DAPI; Thermo Fisher Scientific).
567 The following primary antibodies were used in this study: rabbit anti-EBF1 antibody (1:1000,
568 AB10523; Millipore, Darmstadt, Germany,), mouse anti-MYO7A antibody (1:1000, 138-1;
569 Developmental Studies Hybridoma Bank, Iowa City, IA, USA), rabbit anti-MYO7A antibody

570 (1:1000, 25-6790; Proteus BioSciences, Waltham, MA, USA), goat anti-SOX2 antibody (1:250,
571 AF2018; R&D Systems, Minneapolis, MN, USA), rabbit anti-SOX2 antibody (1:100, 11064-1-
572 AP; Proteintech, Manchester, UK), rabbit anti-VGLUT3 antibody (1:500, 135 203; Synaptic
573 systems, Goettingen, Germany), goat anti-JAG1 antibody (1:500, sc-6011; Santa Cruz, Dallas,
574 TX, USA), mouse anti-p27Kip1 antibody (1:200, 610242; BD Transduction Laboratories), rabbit
575 anti-Tubulin β 3 (TUJ1) antibody (1:1000, PRB-435P; Biolegend, San Diego, CA, USA), rabbit
576 anti-PROX1 antibody (1:500, AB5475; Millipore), rabbit anti-p75 antibody (1:500, AB1554;
577 Millipore), and rabbit anti-cleaved caspase 3 (CC3) antibody (1:400, Asp175; Cell Signaling
578 Technology, Danvers, MA, USA).
579 Antigen retrieval was performed for p27Kip1 staining by heating sections in HistoVT one
580 (Nacalai Tesque) at 90 ℃ for 10 min prior to the addition of the primary antibodies.
581 The secondary antibodies used were Alexa Flour 488 donkey anti-rabbit IgG, Alexa Flour 488
582 donkey anti-goat IgG, Alexa Flour 488 donkey anti-mouse IgG, Alexa Flour 568 donkey anti-
583 rabbit IgG, Alexa Flour 568 donkey anti-goat IgG, Alexa Flour 633 donkey anti-rabbit IgG,
584 Alexa Flour 633 donkey anti-goat IgG, and Alexa Flour 633 donkey anti-mouse IgG (1:500;
585 Thermo Fisher Scientific).
586 The sections were mounted using Fluoromount-G® Anti-Fade (Southern Biotechnology
587 Associates Inc., Birmingham, AL, USA). Images of the specimens were captured using an
588 Olympus BX50 microscope (Olympus), an Olympus DP70 digital camera (Olympus), and a
589 Zeiss LSM900 with Airyscan2 (Carl Zeiss AG, Oberkochen, Germany).
590
591 *HE staining*
592 Frozen sections (10-μm thick) were immersed in Mayer's Hematoxylin Solution (FUJIFILM

Wako Pure Chemical Corporation) at RT for 3 min and in Eosin Alcohol solution (FUJIFILM Wako Pure Chemical Corporation) at RT for 1 min. Dehydration was performed using graded ethanol solutions (70%, 80%, 90%, and 100%) and clearing was performed three times using xylene.

Cochlea whole-mount preparation

The inner ears were dissected from mice heads at E18.5 and fixed in 4% PFA in PBS at RT for 1 h. After fixation and before primary antibody staining, the outer membrane, including the tectorial membrane, was removed to expose the organs of Corti. After staining with a secondary antibody, the organ of Corti was dissected and mounted on a glass slide for imaging.

Proliferation and apoptosis assays

Cell proliferation in the cochlea was assessed by detecting the incorporated EdU (Thermo Fisher Scientific) on frozen sections. EdU was detected using the Click-iT Plus EdU Cell Proliferation Kit for Imaging Alexa 555 Dye (Thermo Fisher Scientific), according to the manufacturer's instructions. Pregnant mice were injected with EdU (Thermo Fisher Scientific) at E12.5, E13.5, and E14.5 (three injections at 50 μg/g at 2-h intervals) and at E16.5 (a single injection at 100 μg/g). E12.5, E13.5, and E14.5 embryos were collected 8 h after the first injection. E16.5 embryos were collected 4 h after the injection. The basal or basal-to-middle regions of the cochlear duct were observed at E12.5 or at E13.5, E14.5, and E16.5, respectively.

Apoptotic cells were detected by identifying the expression of CC3 in frozen sections via IHC staining.

ABR and DPOAE

ABR measurements were performed under general anesthesia as described previously (Kada et al., 2009) at P21 (n = 3 for each genotype). The thresholds for 10, 20, and 40 kHz were determined based on the responses at different intensities with 5 dB sound pressure level intervals. DPOAE recordings were performed as described previously (Hamaguchi et al., 2012) at P21 (n = 4 for each genotype). Two primary tones (f1, f2, f1<f2) were used as input signals, with f2 set at eight frequency points (4, 6, 8, 12, 16, 24, 32, and 40 kHz), maintaining a frequency ratio of f2/f1 = 1.2. The intensity levels of the stimulatory sounds were 65 and 55 dB sound pressure level for f1 and f2, respectively. DPOAE was detected as a peak at 2f1–f2 in the spectrum.

Quantification

Cell quantification and measurements were performed at E18.5 using the Cell Counter plugin of ImageJ (Schneider et al., 2012). The total length of the cochlea was measured based on the region with MYO7A-positive hair cells from the basal to apical turns. Cochlear hair cells were identified by phalloidin and MYO7A labeling. Two types of cells, PROX1- and SOX2-positive cells, were counted to quantify the supporting cells of the cochlea. The cochlear duct was divided into three regions: basal, middle, and apical, and we counted the number of cells per 200 μm in each region for MYO7A- and PROX1-positive cells or 100 μm in the basal region for SOX2-positive cells.

Statistical analysis

For all statistical analyses, at least three samples from each experimental group were analyzed.

Student's *t*-test was used to determine the differences between two experimental groups. One-way or two-way analysis of variance was performed to assess the differences between more than two experimental groups and *p*-values less than 0.05 were considered statistically significant. Statistical analyses were performed using R version 4.2.2 (2022-10-31). All details of statistical analyses are provided in the figures and legends.

Competing Interest Statement

The authors declare that they have no known competing financial interests or personal relationships that could have appeared to influence the work reported in this paper

Acknowledgements

We thank Dr. Rudolf Grosschedl for providing Ebf1$^{-/-}$ and Ebf1$^{fl/fl}$ mice and Dr. Ryoichiro Kageyama for providing *Atoh1* ISH probe. This study was supported by JSPS KAKENHI (grant number: JP22H03234) awarded to NY.

Author Contributions

N.Y. and H.O. designed the study. H.K., H.O., R.Y., and Y.T. performed the experiments with advice from N.Y., T.K., and K.O.. A.Y. performed ABR and DPOAE. H.K. and N.Y. wrote the manuscript with contribution from all authors.

References

661 Bermingham-McDonogh O, Oesterle EC, Stone JS, Hume CR, Huynh HM, Hayashi T (2006)
662 Expression of Prox1 during mouse cochlear development. The Journal of comparative
663 neurology 496:172-186.
664 Bermingham NA, Hassan BA, Price SD, Vollrath MA, Ben-Arie N, Eatock RA, Bellen HJ,
665 Lysakowski A, Zoghbi HY (1999) Math1: an essential gene for the generation of inner
666 ear hair cells. Science 284:1837-1841.
667 Chen P, Segil N (1999) p27(Kip1) links cell proliferation to morphogenesis in the developing
668 organ of Corti. Development 126:1581-1590.
669 Chen P, Johnson JE, Zoghbi HY, Segil N (2002) The role of Math1 in inner ear development:
670 Uncoupling the establishment of the sensory primordium from hair cell fate
671 determination. Development 129:2495-2505.
672 Classon M, Harlow E (2002) The retinoblastoma tumour suppressor in development and cancer.
673 Nature Reviews Cancer 2:910-917.
674 Coate TM, Kelley MW (2013) Making connections in the inner ear: Recent insights into the
675 development of spiral ganglion neurons and their connectivity with sensory hair cells.
676 Seminars in Cell and Developmental Biology 24:460-469.
677 Dayaratne MW, Vlajkovic SM, Lipski J, Thorne PR (2014) Kolliker's organ and the
678 development of spontaneous activity in the auditory system: implications for hearing
679 dysfunction. BioMed research international 2014:367939.
680 Derecka M, Herman JS, Cauchy P, Ramamoorthy S, Lupar E, Grun D, Grosschedl R (2020)
681 EBF1-deficient bone marrow stroma elicits persistent changes in HSC potential. Nature
682 immunology 21:261-273.
683 Ebeid M, Barnas K, Zhang H, Yaghmour A, Noreikaite G, Bjork BC (2022) PRDM16
684 expression and function in mammalian cochlear development. Developmental Dynamics.
685 Ferri A, Favaro R, Beccari L, Bertolini J, Mercurio S, Nieto-Lopez F, Verzeroli C, La Regina F,
686 De Pietri Tonelli D, Ottolenghi S, Bovolenta P, Nicolis SK (2013) Sox2 is required for
687 embryonic development of the ventral telencephalon through the activation of the ventral
688 determinants Nkx2.1 and Shh. Development 140:1250-1261.
689 Fretz JA, Nelson T, Velazquez H, Xi Y, Moeckel GW, Horowitz MC (2014) Early B-cell factor
690 1 is an essential transcription factor for postnatal glomerular maturation. Kidney
691 International 85:1091-1102.
692 Garel S, Garcia-Dominguez M, Charnay P (2000) Control of the migratory pathway of facial
693 branchiomotor neurones. Development 127:5297-5307.
694 Garel S, Marin F, Grosschedl R, Charnay P (1999) Ebf1 controls early cell differentiation in the
695 embryonic striatum. Development 126:5285-5294.
696 Gyory I, Boller S, Nechanitzky R, Mandel E, Pott S, Liu E, Grosschedl R (2012) Transcription
697 factor Ebf1 regulates differentiation stage-specific signaling, proliferation, and survival
698 of B cells. Genes and Development 26:668-682.
699 Hagman J, Travis A, Grosschedl R (1991) A novel lineage-specific nuclear factor regulates mb-1
700 gene transcription at the early stages of B cell differentiation. The EMBO journal
701 10:3409-3417.
702 Hagman J, Gutch MJ, Lin H, Grosschedl R (1995) EBF contains a novel zinc coordination motif
703 and multiple dimerization and transcriptional activation domains. EMBO Journal
704 14:2907-2916.

705 Hamaguchi K, Yamamoto N, Nakagawa T, Furuyashiki T, Narumiya S, Ito J (2012) Role of
706 PGE-type receptor 4 in auditory function and noise-induced hearing loss in mice.
707 Neuropharmacology 62:1841-1847.
708 Hébert JM, McConnell SK (2000) Targeting of cre to the Foxg1 (BF-1) locus mediates loxP
709 recombination in the telencephalon and other developing head structures. Developmental
710 Biology 222:296-306.
711 Hesslein DG, Fretz JA, Xi Y, Nelson T, Zhou S, Lorenzo JA, Schatz DG, Horowitz MC (2009)
712 Ebf1-dependent control of the osteoblast and adipocyte lineages. Bone 44:537-546.
713 Jimenez MA, Akerblad P, Sigvardsson M, Rosen ED (2007) Critical role for Ebf1 and Ebf2 in
714 the adipogenic transcriptional cascade. Molecular and Cellular Biology 27:743-757.
715 Jin K, Xiang M (2011) Ebf1 deficiency causes increase of Müller cells in the retina and
716 abnormal topographic projection at the optic chiasm. Biochemical and Biophysical
717 Research Communications 414:539-544.
718 Jin K, Jiang H, Mo Z, Xiang M (2010) Early B-cell factors are required for specifying multiple
719 retinal cell types and subtypes from postmitotic precursors. The Journal of neuroscience :
720 the official journal of the Society for Neuroscience 30:11902-11916.
721 Kada S, Nakagawa T, Ito J (2009) A Mouse Model for Degeneration of the Spiral Ligament.
722 Journal of the Association for Research in Otolaryngology 10:161-172.
723 Kiernan AE, Pelling AL, Leung KKH, Tang ASP, Bell DM, Tease C, Lovell-Badge R, Steel KP,
724 Cheah KSE (2005) Sox2 is required for sensory organ development in the mammalian
725 inner ear. Nature 434:1031-1035.
726 Kolla L, Kelly MC, Mann ZF, Anaya-Rocha A, Ellis K, Lemons A, Palermo AT, So KS, Mays
727 JC, Orvis J, Burns JC, Hertzano R, Driver EC, Kelley MW (2020) Characterization of the
728 development of the mouse cochlear epithelium at the single cell level. Nature
729 communications 11:2389.
730 Kubota M, Scheibinger M, Jan TA, Heller S (2021) Greater epithelial ridge cells are the principal
731 organoid-forming progenitors of the mouse cochlea. Cell Reports 34:108646.
732 Li C, Shu Y, Wang G, Zhang H, Lu Y, Li X, Li G, Song L, Liu Z (2018) Characterizing a novel
733 vGlut3-P2A-iCreER knockin mouse strain in cochlea. Hear Res 364:12-24.
734 Liberg D, Sigvardsson M, Akerblad P (2002) The EBF/Olf/Collier family of transcription
735 factors: regulators of differentiation in cells originating from all three embryonal germ
736 layers. Molecular and Cellular Biology 22:8389-8397.
737 Lin H, Grosschedl R (1995) Failure of B-cell differentiation in mice lacking the transcription
738 factor EBF. Nature 376:263-267.
739 Lipinski MM, Jacks T (1999) The retinoblastoma gene family in differentiation and development.
740 Oncogene 18:7873-7882.
741 Mason HA, Rakowiecki SM, Raftopoulou M, Nery S, Huang Y, Gridley T, Fishell G (2005)
742 Notch signaling coordinates the patterning of striatal compartments. Development
743 132:4247-4258.
744 Nechanitzky R, Akbas D, Scherer S, Gyory I, Hoyler T, Ramamoorthy S, Diefenbach A,
745 Grosschedl R (2013) Transcription factor EBF1 is essential for the maintenance of B cell
746 identity and prevention of alternative fates in committed cells. Nature immunology
747 14:867-875.
748 Nelson T, Velazquez H, Troiano N, Fretz JA (2019) Early B Cell Factor 1 (EBF1) Regulates
749 Glomerular Development by Controlling Mesangial Maturation and Consequently COX-
750 2 Expression. Journal of the American Society of Nephrology : JASN 30:1559-1572.

751 Nieminen-Pihala V, Tarkkonen K, Laine J, Rummukainen P, Saastamoinen L, Nagano K, Baron
752 R, Kiviranta R (2021) Early B-cell Factor1 (Ebf1) promotes early osteoblast
753 differentiation but suppresses osteoblast function. Bone 146:115884.
754 Ohyama T, Basch ML, Mishina Y, Lyons KM, Segil N, Groves AK (2010) BMP Signaling Is
755 Necessary for Patterning the Sensory and Nonsensory Regions of the Developing
756 Mammalian Cochlea. Journal of Neuroscience 30:15044-15051.
757 Phippard D, Lu L, Lee D, Saunders JC, Crenshaw EB, 3rd (1999) Targeted mutagenesis of the
758 POU-domain gene Brn4/Pou3f4 causes developmental defects in the inner ear. The
759 Journal of neuroscience : the official journal of the Society for Neuroscience 19:5980-
760 5989.
761 Ruijtenberg S, van den Heuvel S (2016) Coordinating cell proliferation and differentiation:
762 Antagonism between cell cycle regulators and cell type-specific gene expression. Cell
763 Cycle 15:196-212.
764 Sage C, Huang M, Karimi K, Gutierrez G, Vollrath MA, Zhang DS, Garcia-Anoveros J, Hinds
765 PW, Corwin JT, Corey DP, Chen ZY (2005) Proliferation of functional hair cells in vivo
766 in the absence of the retinoblastoma protein. Science 307:1114-1118.
767 Schneider CA, Rasband WS, Eliceiri KW (2012) NIH Image to ImageJ: 25 years of image
768 analysis. Nat Methods 9:671-675.
769 Shen Z, Chen Y, Li L, Liu L, Peng M, Chen X, Wu X, Sferra TJ, Wu M, Lin X, Cheng Y, Chu J,
770 Shen A, Peng J (2020) Transcription Factor EBF1 Over-Expression Suppresses Tumor
771 Growth in vivo and in vitro via Modulation of the PNO1/p53 Pathway in Colorectal
772 Cancer. Front Oncol 10:1035.
773 Sher AE (1971) The embryonic and postnatal development of the inner ear of the mouse. Acta
774 oto-laryngologica Supplementum 285:1-77.
775 Taniguchi M, Yamamoto N, Nakagawa T, Ogino E, Ito J (2012) Identification of tympanic
776 border cells as slow-cycling cells in the cochlea. PloS one 7:e48544.
777 Urness LD, Wang X, Shibata S, Ohyama T, Mansour SL (2015) Fgf10 is required for
778 specification of non-sensory regions of the cochlear epithelium. Developmental Biology
779 400:59-71.
780 von Bartheld CS, Patterson SL, Heuer JG, Wheeler EF, Bothwell M, Rubel EW (1991)
781 Expression of nerve growth factor (NGF) receptors in the developing inner ear of chick
782 and rat. Development 113:455-470.
783 Wang MM, Reed RR (1993) Molecular cloning of the olfactory neuronal transcription factor
784 Olf-1 by genetic selection in yeast. Nature 364:121-126.
785 Wang SS, Tsai RY, Reed RR (1997) The characterization of the Olf-1/EBF-like HLH
786 transcription factor family: implications in olfactory gene regulation and neuronal
787 development. Journal of Neuroscience 17:4149-4158.
788 Wu DK, Kelley MW (2012) Molecular mechanisms of inner ear development. Cold Spring
789 Harbor Perspectives in Biology 4:a008409.
790 Yamamoto N, Chang W, Kelley MW (2011) Rbpj regulates development of prosensory cells in
791 the mammalian inner ear. Developmental Biology 353:367-379.
792 Yamamoto R, Ohnishi H, Omori K, Yamamoto N (2021) In silico analysis of inner ear
793 development using public whole embryonic body single-cell RNA-sequencing data.
794 Developmental Biology 469:160-171.
795

796

797 **Figures and Figure Legends**

798 **Fig. 1. Quantitative and spatiotemporal expression of *Ebf1* during inner ear development.**

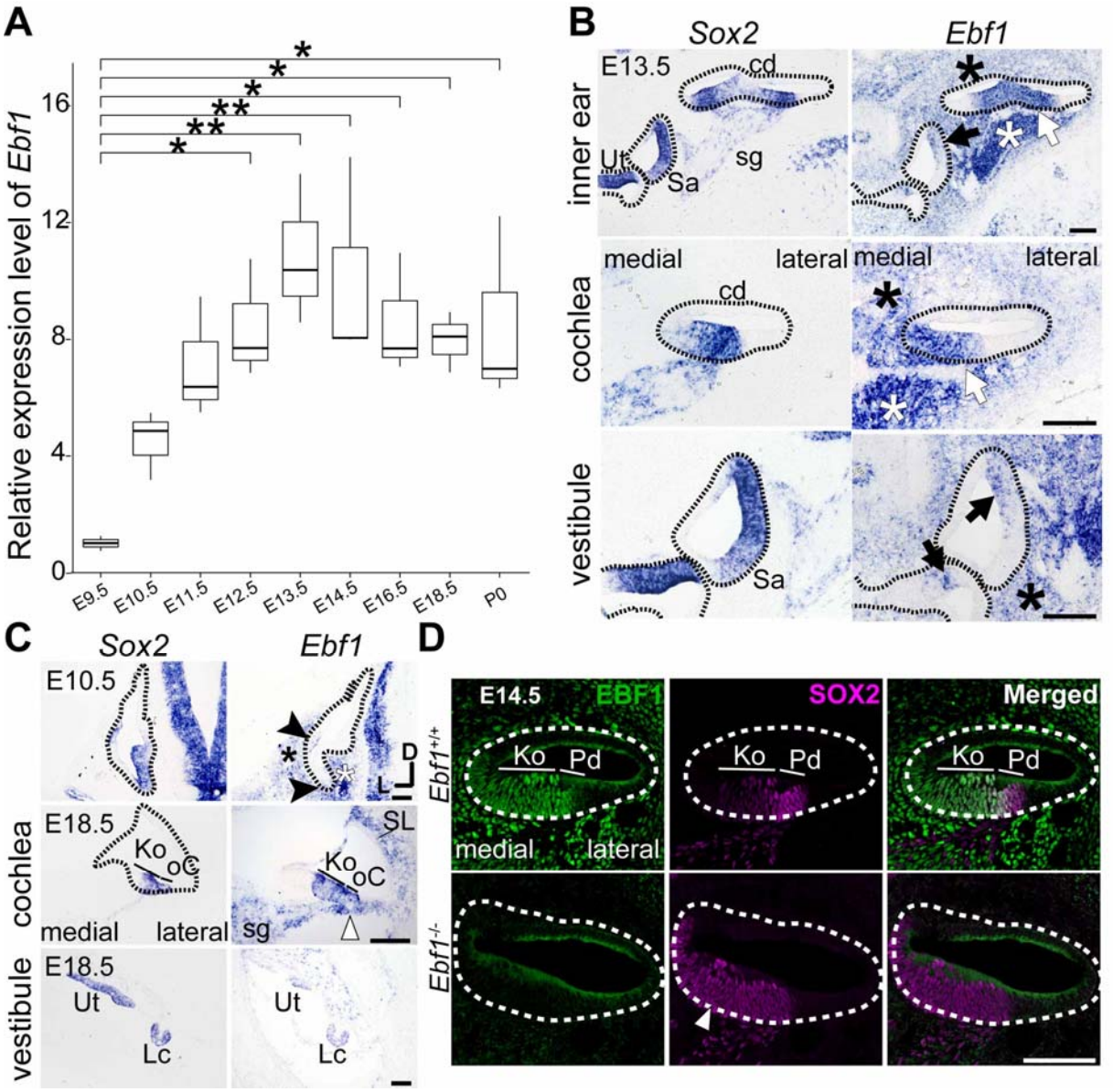

799 **A.** Results of quantitative reverse transcription polymerase chain reaction (qRT-PCR) analysis
800 for *Ebf1* in the inner ear of wild-type mice from embryonic day (E) 9.5 to P0. The value of each
801 date is normalized to the value of E9.5. Box plot representing the medians and interquartile
802 ranges of the relative mRNA expression of *Ebf1*.

B and **C**. Result of *in situ* hybridization for *Ebf1* and *Sox2* in cross sections of the inner ear of wild-type mice at E13.5 (B) and E10.5 and E18.5 (C). Areas enclosed by dashed lines indicate the inner ear epithelium. Low-magnification images of the cochlear basal turn and vestibule are presented in the uppermost panels of **B**. High-magnification images of the apical turn of the cochlear duct and vestibules are presented in the middle and lower panels of **B**. Images of E10.5 otocysts and E18.5 cochleae and vestibules are presented in the uppermost, middle, and lowermost images of **C**, respectively.

D. Immunohistochemical images of E14.5 $Ebf1^{+/+}$ (upper panels) and $Ebf1^{-/-}$ (lower panels) mouse cochlear ducts.

One-way analysis of variance (ANOVA) with Tukey–Kramer *post-hoc* tests was performed. $*p < 0.05$, $**p < 0.01$. D, dorsal; L, lateral. cd, cochlear duct; sg, spiral ganglion; Ut, utricle; Sa, saccule; Lc, lateral crista; SL, spiral ligament; Ko, Kölliker's organ; oC, organ of Corti; Pd, prosensory domain. Scale bars: 100 μm.

817 **Fig. 2 Development of the cochlear duct is deteriorated in *Ebf1*$^{-/-}$ mice.**

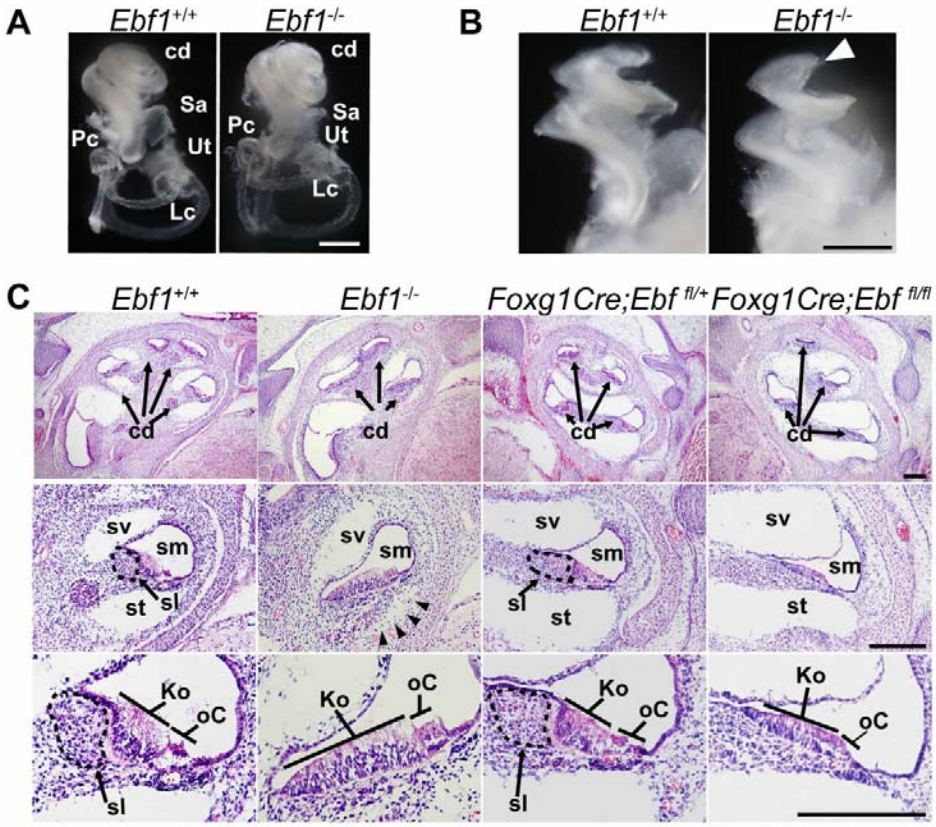

818 **A.** Gross morphology of membranous labyrinth of the inner ear of *Ebf1*$^{+/+}$ and *Ebf1*$^{-/-}$mice at
819 embryonic day (E) 18.5. **B.** Gross morphology of the cochlear floor after the lateral wall and roof
820 of the cochlea were removed at E18.5. **C.** Hematoxylin and eosin-stained cross sections of the
821 cochlea at E18.5 from *Ebf1*$^{+/+}$, *Ebf1*$^{-/-}$, *Foxg1Cre;Ebf1*$^{fl/+}$, and *Foxg1Cre;Ebf1*$^{fl/fl}$ mice. The
822 upper panels are low-magnification images, and the middle and lower panels are high-
823 magnification images. Areas enclosed by dashed lines indicate the spiral limbus. cd, cochlear
824 duct; Ut, utricle; Sa, saccule; Lc, lateral crista; Pc, posterior crista; sv, scala vestibuli; sm, scala
825 media; st, scala tympani; sl, spiral limbus: Ko, Kölliker's organ; oC, organ of Corti. Scale bars:
826 0.5 mm in **A** and **B** and 200 μm in **C**.

827

828 **Fig. 3. *Ebf1* deletion increases the number of MYO7A-, SOX2-, and PROX1-positive cells**

829 **in the cochlea.**

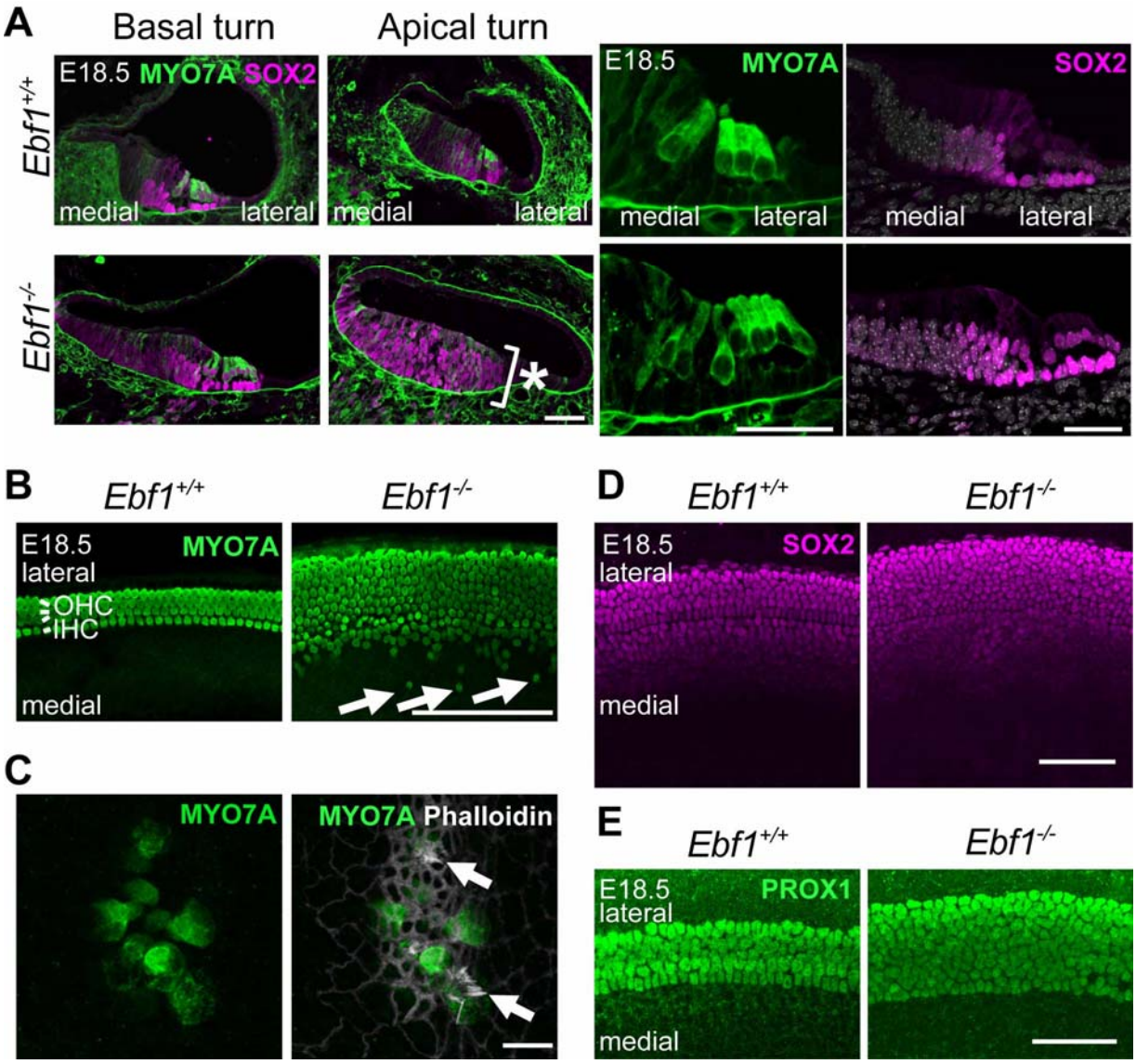

830

831 **A.** Cross sections of the basal and apical turns of the cochlea of *Ebf1*$^{+/+}$ and *Ebf1*$^{-/-}$ mice at

832 embryonic day (E) 18.5, labeled with MYO7A (green) and SOX2 (magenta). Magnified images

833 of the organ of Corti (oC) and Kölliker's organ (Ko) are presented in the four right panels. **B**–**E**.

834 Whole mount cochlear images from *Ebf1*$^{+/+}$ and *Ebf1*$^{-/-}$ mice at E18.5, labeled with MYO7A

835 (green, **B** and **C**), phalloidin (white, **C**), SOX2 (magenta, **D**), and PROX1 (green, **E**). Scale bars:

836 50 μm in **A**, **D**, and **E**; 100 μm in **B**; 10 μm in **C**.

837

838 **Fig. 4. Increases in the number of hair and supporting cells.**

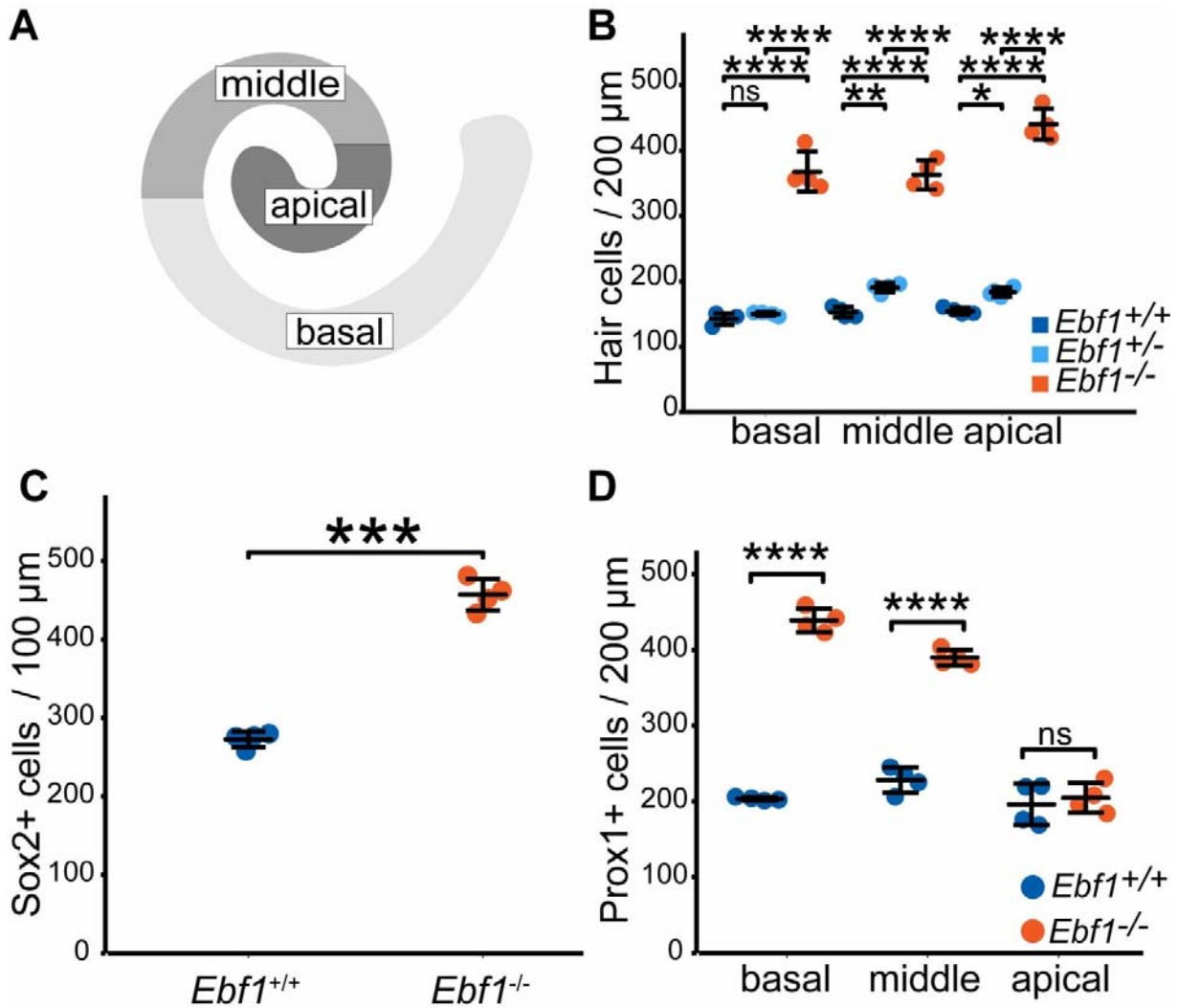

839

840 **A**. Schematic diagram of the cochlea duct showing the positions of the basal, middle, and apical
841 regions of the cochlea. **B**. Total hair cell numbers per 200 µm in the basal, middle, and apical
842 regions of the cochlear ducts of *Ebf1*$^{+/+}$, *Ebf1*$^{+/-}$, and *Ebf1*$^{-/-}$ mice at embryonic day (E) 18.5. **C**.
843 Numbers of SOX2-positive cells per 100 µm in the basal region of the cochlea. **D**. Numbers of
844 PROX1-positive cells per 200 µm in the basal, middle, and apical regions of the cochlea. Two-
845 way analysis of variance (ANOVA) test with Bonferroni *post-hoc* test (**B** and **D**) and Student's *t*-

846 test (**C**) were performed. *$p < 0.05$, **$p < 0.01$, ***$p < 0.001$, and ****$p < 0.0001$; ns, not

847 significant. Error bars represent mean ± standard deviation (n = 4).

848

Fig. 5. *Ebf1* deletion causes JAG1 expression to spread inward, delaying *Atoh1* expression during cochlear development.

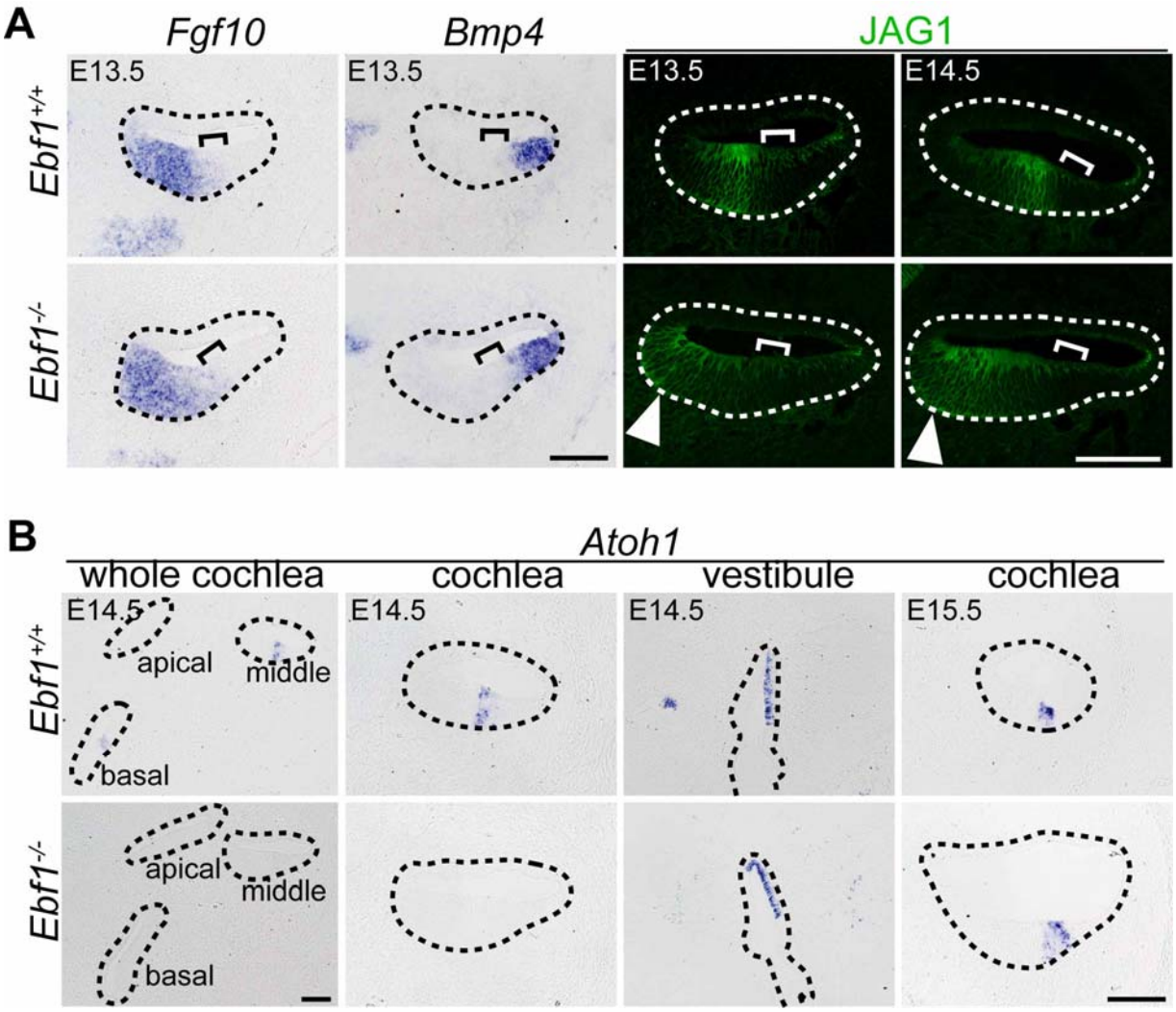

A. Results of *in situ* hybridization of *Fgf10* and *Bmp4* and immunostaining of JAG1 (green) on cross sections of the basal-to-middle region of the cochlea of *Ebf1*$^{+/+}$ and *Ebf1*$^{-/-}$ mice at embryonic day (E) 13.5 and E14.5. The prosensory domain is shown in brackets. **B**. Result of *in situ* hybridization of *Atoh1* on cross sections of the basal-to-middle region of the cochlea of *Ebf1*$^{+/+}$ and *Ebf1*$^{-/-}$ mice at E14.5 and E15.5. Areas enclosed by dashed lines indicate cochlear ducts and vestibules. Scale bars: 100 μm.

858

859 **Fig. 6. Effect of *Ebf1* deletion on cell proliferation during inner ear development.**

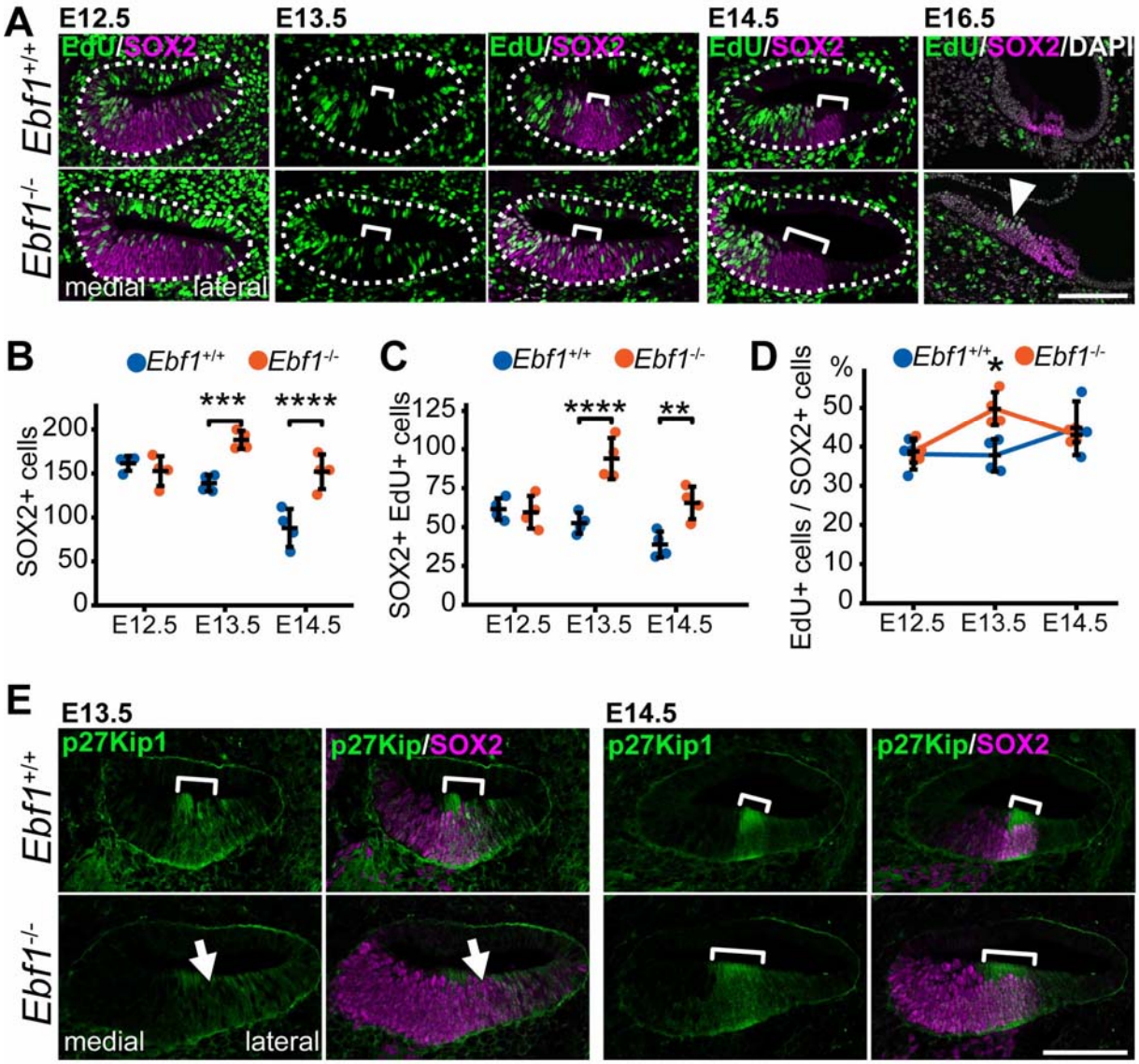

860

861 **A**. Cross sections of the cochlear basal regions at embryonic day (E) 12.5, E13.5, E14.5, and
862 E16.5 from *Ebf1*$^{+/+}$ and *Ebf1*$^{-/-}$ mice. Sections were immunostained with 5-ethynyl-2'-
863 deoxyuridine (EdU, green) and SOX2 (magenta). E16.5 sections were counter-stained with 4',6-
864 diamidino-2-phenylindole (DAPI, gray). Areas enclosed by dashed lines indicate the cochlear
865 ducts and brackets indicate prosensory domains. **B**–**D**. Quantitative assessment of the SOX2-

positive region in the cochlea epithelia. The numbers of SOX2-positive cells (**B**) as well as EdU- and SOX2-double positive cells (**C**) were counted, and the percentage of EdU-positive cells among SOX2-positive cells (**D**) was calculated. *$p < 0.05$, **$p < 0.01$, ***$p < 0.001$, and ****$p < 0.0001$. Error bars represent mean ± standard deviation. n = 4. **E**. Cross sections of the cochlear basal regions at E13.5 and E14.5 from *Ebf1*$^{+/+}$ and *Ebf1*$^{-/-}$ mice immunostained with p27Kip1 (green) and SOX2 (magenta). Scale bars: 100 μm.

873 **Fig. 7. *Ebf1* deletion impairs auditory function.**

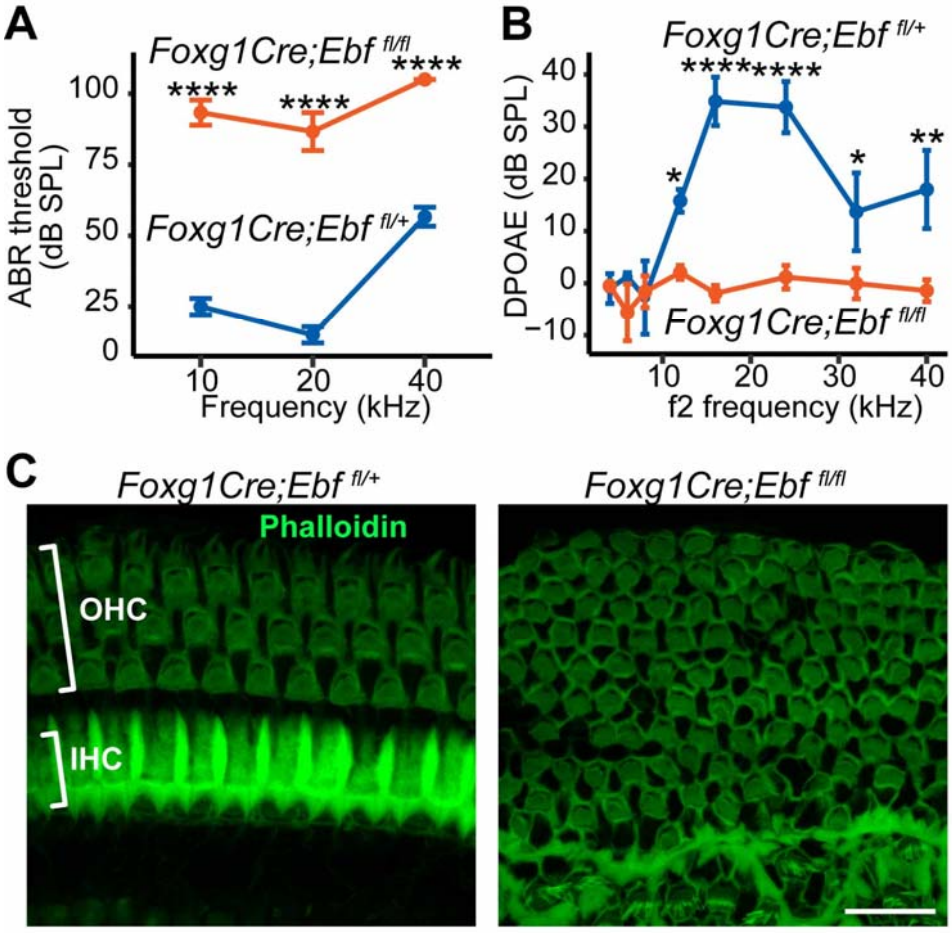

874

875 **A**. Auditory brainstem response (ABR) thresholds of P21 *Foxg1Cre;Ebf1*$^{fl/fl}$ (red) and
876 *Foxg1Cre;Ebf1*$^{fl/+}$ (blue, control) mice. **B**. Distortion product optoacoustic emissions (DPOAE)
877 were measured at P21 from *Foxg1Cre;Ebf1*$^{fl/fl}$ (red) and control (blue) mice. *$p < 0.05$, **$p <$
878 0.01, and ****$p < 0.0001$ from one-way analysis of variance (ANOVA) with Tukey's HSD *post-*
879 *hoc* test. Error bars represent mean ± standard error of mean. **C**. The whole mount images of the
880 cochlear basal regions from *Foxg1Cre;Ebf1*$^{fl/+}$ and *Foxg1Cre;Ebf1*$^{fl/fl}$ mice at P23 labeled with
881 phalloidin (green). Scale bar: 20 μm.

882

883 **Supplemental Figures and Legends for Supplemental Figures**

884 **Supplemental Fig. S1. Spatiotemporal expression of *Ebf1* during inner ear development.**

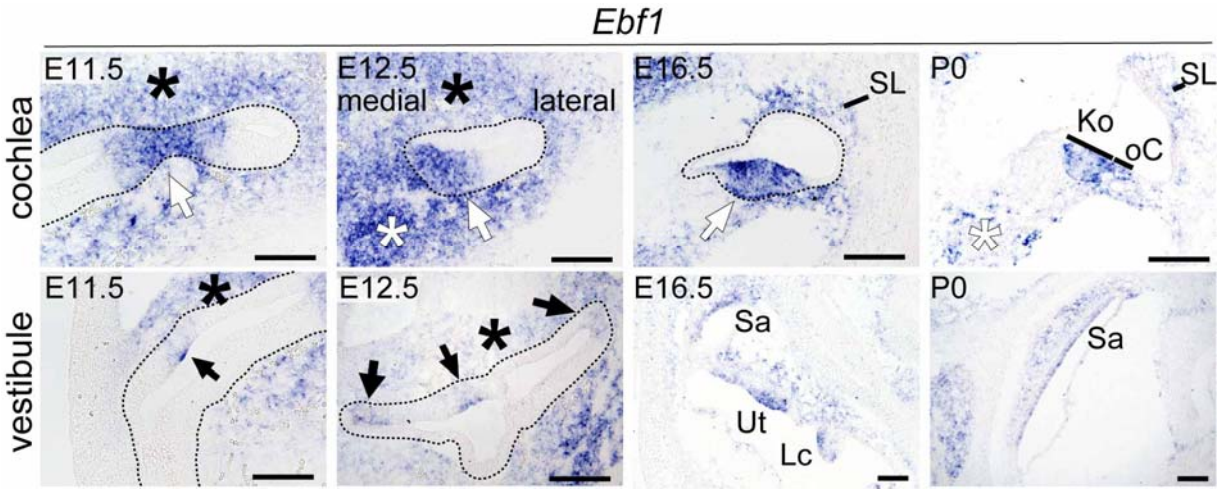

885

886 Result of *in situ* hybridization for *Ebf1* and *Sox2* on cross sections of the inner ear of wild-type
887 mice at embryonic day (E) 11.5, E12.5, E16.5, and P0. Areas enclosed by dashed lines indicate
888 the inner ear epithelium. From E11.5 to P0, *Ebf1* is expressed in the sensory epithelium of the
889 cochlea (white arrows), the vestibular and semicircular canals (arrows), the spiral ganglion
890 (white asterisks), and the surrounding mesenchymal tissues (asterisks and SL). sg, spiral
891 ganglion; Ut, utricle; Sa, saccule; Lc, lateral crista; SL, spiral ligament; Ko, Kölliker's organ; oC,
892 organ of Corti. Scale bars: 100 μm.

893

894 **Supplemental Fig. S2. *Ebf1* deletion does not affect hair and supporting cells in the**

895 **vestibular macula and crista.**

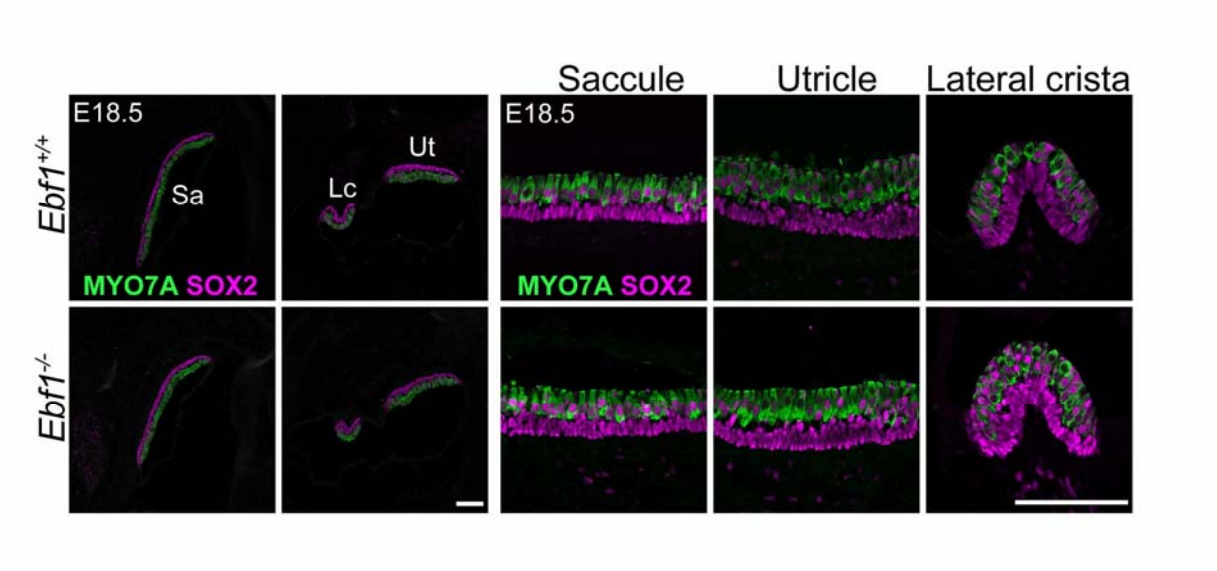

896

897 Cross sections of the embryonic day (E) 18.5 vestibular region immunostained for MYO7A

898 (green) and SOX2 (magenta). Low-magnification (left four panels) and high-magnification (right

899 panels) images of the saccule, lateral crista, and utricle are presented. Ut, utricle; Sa, saccule; Lc,

900 lateral crista. Scale bars: 100 μm.

901

902 **Supplemental Fig. S3. *Ebf1* deletion causes increased number of inner hair cells and**

903 **delayed differentiation of hair and supporting cells.**

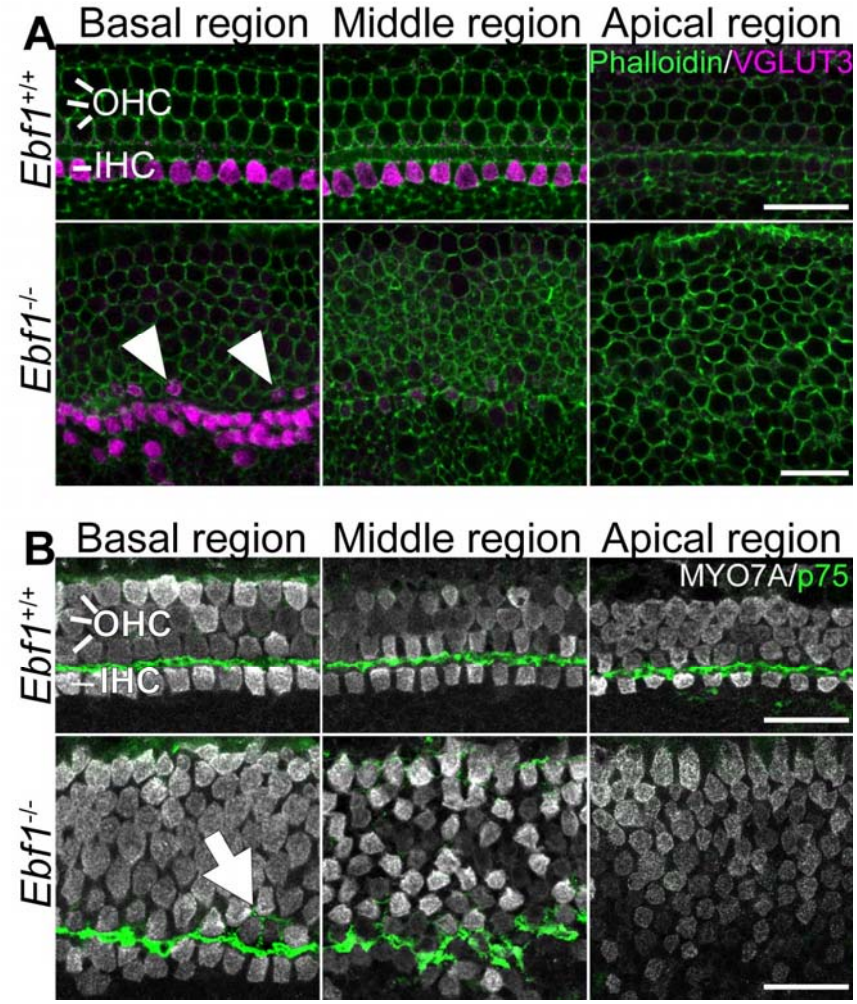

904

905 High-magnification images of the basal, middle, and apical regions of whole-mount cochlear

906 samples from E18.5 *Ebf1*$^{+/+}$ and *Ebf1*$^{-/-}$ mice. **A**. Immunostaining with phalloidin (green) and an

907 anti-VGLUT3 antibody (magenta). In the cochlea of *Ebf1*$^{-/-}$ mice, the row number of VGLUT3-

908 positive cells was 2 to 3, whereas this number was only 1 in wild-type mice. VGLUT3-positive

909 cells were observed only in the basal region of the cochlea but not in the middle and apical

910 regions of *Ebf1*$^{-/-}$ mice. Several VGLUT3-positive cells were observed in the outer hair cell area

911 (arrowheads). **B**. Immunostaining with anti-MYO7A (gray) and p75 (green) antibodies. In the

912 cochlea of *Ebf1*$^{-/-}$ mice, the row number of p75-positive cells was similar to that in *Ebf1*$^{+/+}$ mice,
913 although their arrangement was deteriorated in *Ebf1*$^{-/-}$ mice (arrow**)**. p75-positive cells are
914 observed only in the basal and middle region in the *Ebf1*$^{-/-}$ mice. Scale bars: 20 μm.
915

916 **Supplemental Fig. S4. Quantification of cochlear length.**

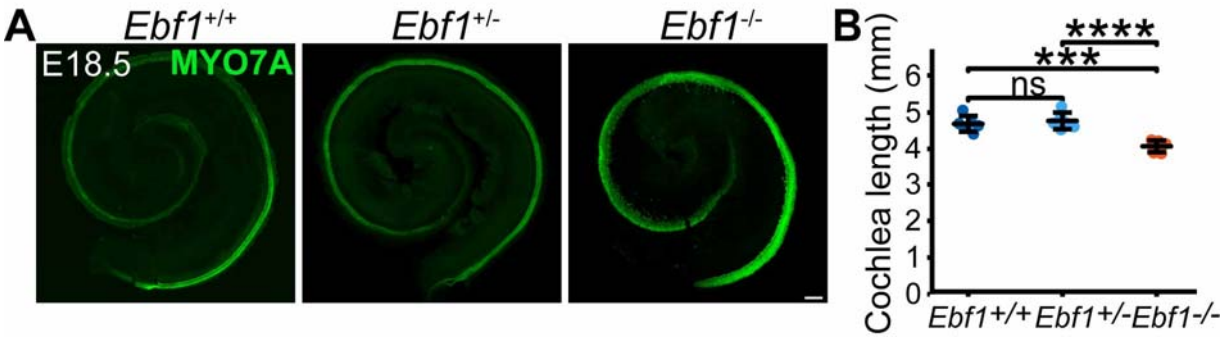

917

918 **A**. Whole mount images of the cochlea of embryonic day (E) 18.5 *Ebf1*$^{+/+}$, *Ebf1*$^{+/-}$, and *Ebf1*$^{-/-}$

919 mice labeled with MYO7A (green). **B**. Quantification of cochlear duct length of E18.5 *Ebf1*$^{+/+}$,

920 *Ebf1*$^{+/-}$, and *Ebf1*$^{-/-}$ mice. The cochlear length of *Ebf1*$^{-/-}$ mice was significantly shorter than those

921 of *Ebf1*$^{+/+}$and *Ebf1*$^{+/-}$ mice. Two-way analysis of variance (ANOVA) test with Bonferroni *post-*

922 *hoc* tests was performed. ***$p < 0.001$, and ****$p < 0.0001$; ns, not significant. Error bars

923 represent mean ± standard deviation. n = 6

924

925 **Supplemental Fig. S5. *Ebf1* deletion causes aberrant spiral ganglion development and axon**

926 **outgrowth to cochlear hair cells.**

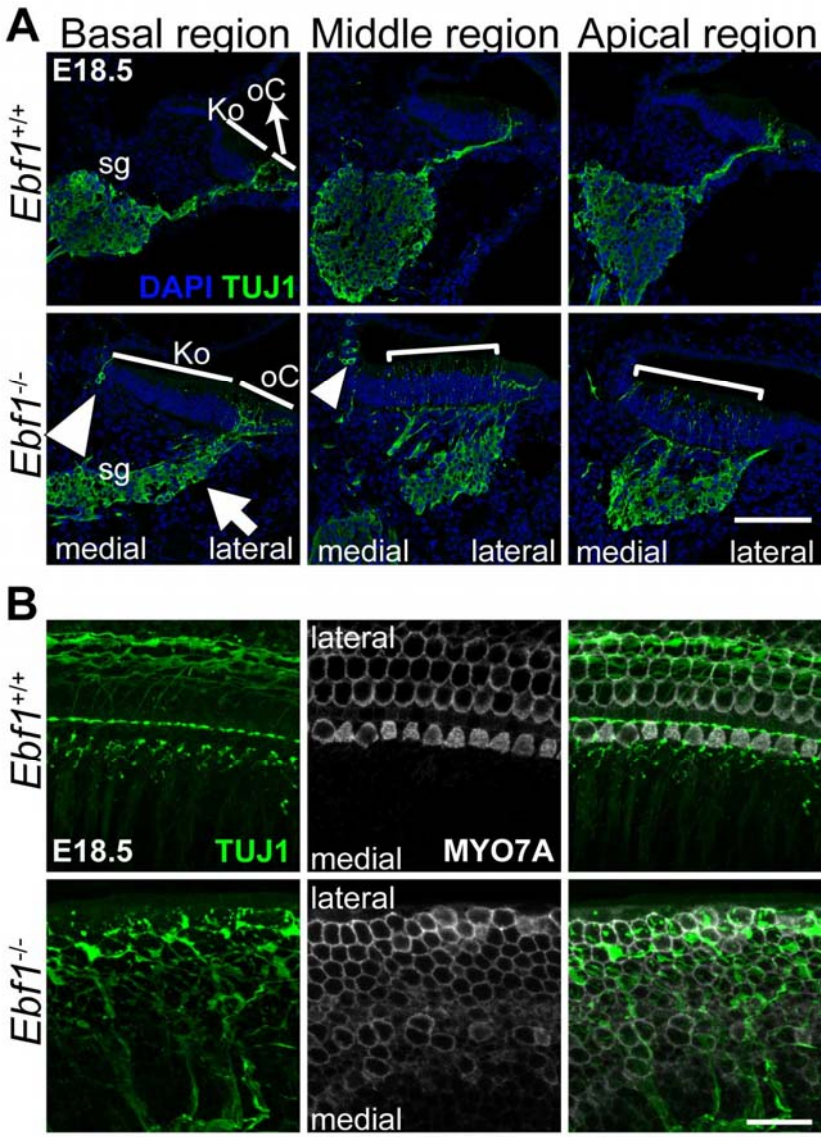

927

928 **A**. Cross sections of the basal, middle, and apical regions of the cochlea and spiral ganglion in

929 embryonic day (E) 18.5 *Ebf1*$^{+/+}$ and *Ebf1*$^{-/-}$ mice stained with Tubulin β 3 (TUJ1, green) and

930 4',6-diamidino-2-phenylindole (DAPI, gray). The morphology of the spiral ganglion in *Ebf1*$^{-/-}$

931 mice differed from that in *Ebf1*$^{+/+}$ mice. TUJ1-positive cell bodies were observed below the

932 organ of Corti (arrow) and at their normal site. Additionally, innervation from the spiral ganglion

933 was observed in the hair cell part and in Kölliker's organ in the middle and apical of the cochlea
934 (arrowheads and brackets). **B**. High-magnification view of the basal region of the whole mount
935 cochlear image in E18.5 *Ebf1*$^{+/+}$ and *Ebf1*$^{-/-}$ mice labeled with TUJ1 (green) and MYO7A (gray).
936 In *Ebf1*$^{+/+}$ mice, the neurons ran parallel to the outer hair cells, whereas in *Ebf1*$^{-/-}$ mice, the
937 neurons formed a reticulation within the cochlear hair cell regions. Scale bars: 100 μm (**A**) and
938 20 μm **(B**).
939

940 **Supplemental Fig. S6. *Ebf1* deletion did not affect apoptosis during inner ear development.**

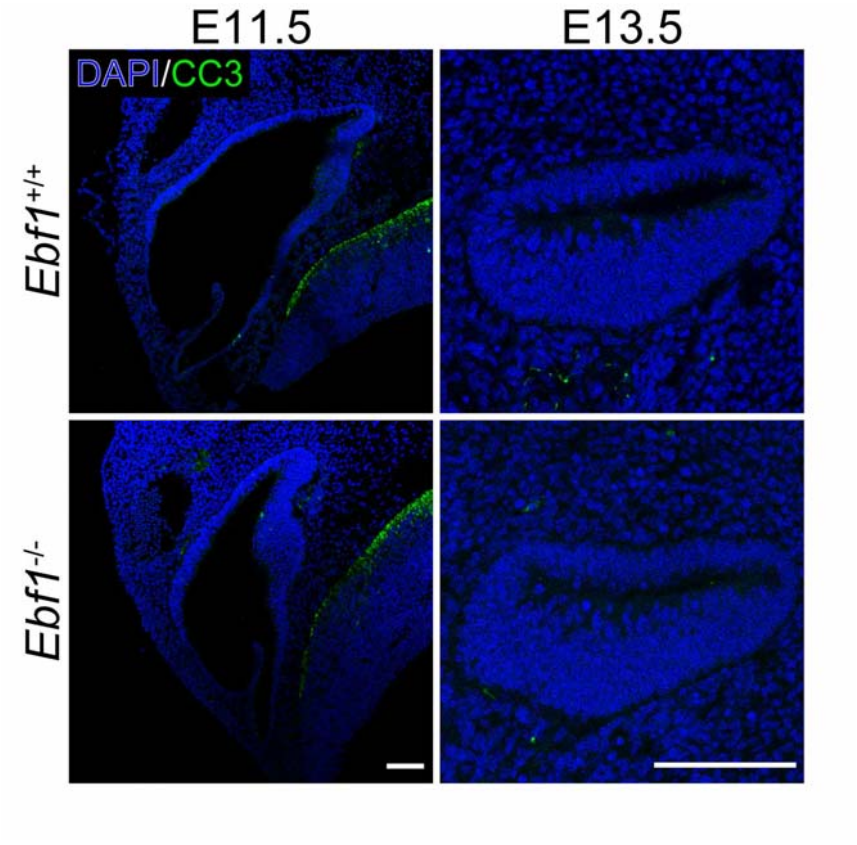

941

942 Cross sections of the embryonic day (E) 11.5 inner ear and E13.5 cochlear basal region from
943 *Ebf1*$^{+/+}$ and *Ebf1*$^{-/-}$ mice. Sections were labeled with cleaved caspase 3 (CC3, green) and 4',6-
944 diamidino-2-phenylindole (DAPI, blue). The number of CC3-positive cells was similar between
945 *Ebf1*$^{-/-}$ and *Ebf1*$^{+/+}$ mice at E11.5 and E13.5. Scale bars: 100 μm.

946